

Figure 4. Neurone navigator 3 (NAV3) protein expression levels in the brains of neurodegenerative diseases. The expression of NAV3 protein was studied in frozen frontal cortex tissues of non-neurological controls (NC), amyotrophic lateral sclerosis (ALS), Parkinson disease (PD) and Alzheimer disease (AD) by Western blot. The panels (a, b) indicate (a) NAV3 protein and (b) 14-3-3 protein, an internal control for protein loading. The lanes (1–21) represent (1–4) NC, (5–10) ALS, (11–14) PD and (15–21) AD. Eighty micrograms of protein was loaded in each lane.

line with these, we identified a panel of extracellular matrix components, such as fibrillin 1, collagen, type V, alpha 3, collagen, type XI, alpha 1 and collagen, type I, alpha 2, as a group of top-ranking miR-29a target genes. The levels of expression of the miR-29 family are reduced in lung cancer, cholangiocarcinoma, chronic lymphocytic leukemia and neuroblastoma, suggesting that miR-29 acts as a proapoptotic anti-oncomir [25–27]. The oncogenic transcription factor cMyc reduces the expression of miR-29 in cancer cells by binding directly to the miR-29 promoter region [28]. By suppressing the expression of PI3 kinase p85 α and CDC42, miR-29 activates p53 and induces apoptosis in HeLa cells [29]. miR-29 acts as an enhancer of myogenic differentiation and a suppressor of rhabdomyosarcoma by targeting YY1 transcription factor [30]. miR-29a promotes the epithelial-to-mesenchymal transition of breast cancer cells by suppressing the expression of tristetruprolin [31]. All of these observations suggest that miR-29a modulates cellular differentiation and survival by regulating a wide range of target mRNAs.

Neurone navigator 3 is a member of the neurone navigator protein family expressed predominantly in the central and peripheral nervous systems [20]. In adult mouse brain, NAV3 is expressed chiefly in nuclear membranes of neurones in the cerebral cortex, midbrain, cerebellum and the hippocampal formation [20]. The NAV3 protein structure is characterized by an N-terminal calponin homology domain, several coiled-coil regions, an actin-binding domain, a GTP/ATP-binding domain and

an AAA-type ATPase domain [32]. Although the biological function of mammalian NAV3 protein in the brain remains totally unknown, a *Caenorhabditis elegans* gene named unc-53 highly homologous to NAV3, plays a key role in axon guidance [33]. Importantly, NAV2, a paralog of NAV3, plays a central role in neurite outgrowth and axonal elongation in human neuroblastoma cells [34]. Furthermore, the NAV3 gene is occasionally disrupted in primary cutaneous T cell lymphomas by chromosomal translocation, suggesting that NAV3 acts as a tumour suppressor gene [35].

We found that the levels of NAV3 mRNA were elevated in AD brains, although we did not find a correlation between NAV3 mRNA levels by real-time RT-PCR and protein levels by Western blot. The lack of the correlation between mRNA levels and protein abundance might be in part attributable to the differential stability and turnover of mRNA and protein via various post-transcriptional mechanisms, including the selective degradation of proteins by proteasome and autophagosome machineries [36]. Nevertheless, we found that pyramidal neurones in the cerebral cortex expressed strong NAV3 immunoreactivity in both AD and non-AD brains. Furthermore, a substantial population of cortical pyramidal neurones coexpressed NAV3 and neurofibrillary tangles in AD brains, where NAV3 immunoreactivity was the most intense in neurones with degenerating morphology bearing pyknotic nuclei. A previous study performed on mouse brains showed that NAV3 immunoreactivity is

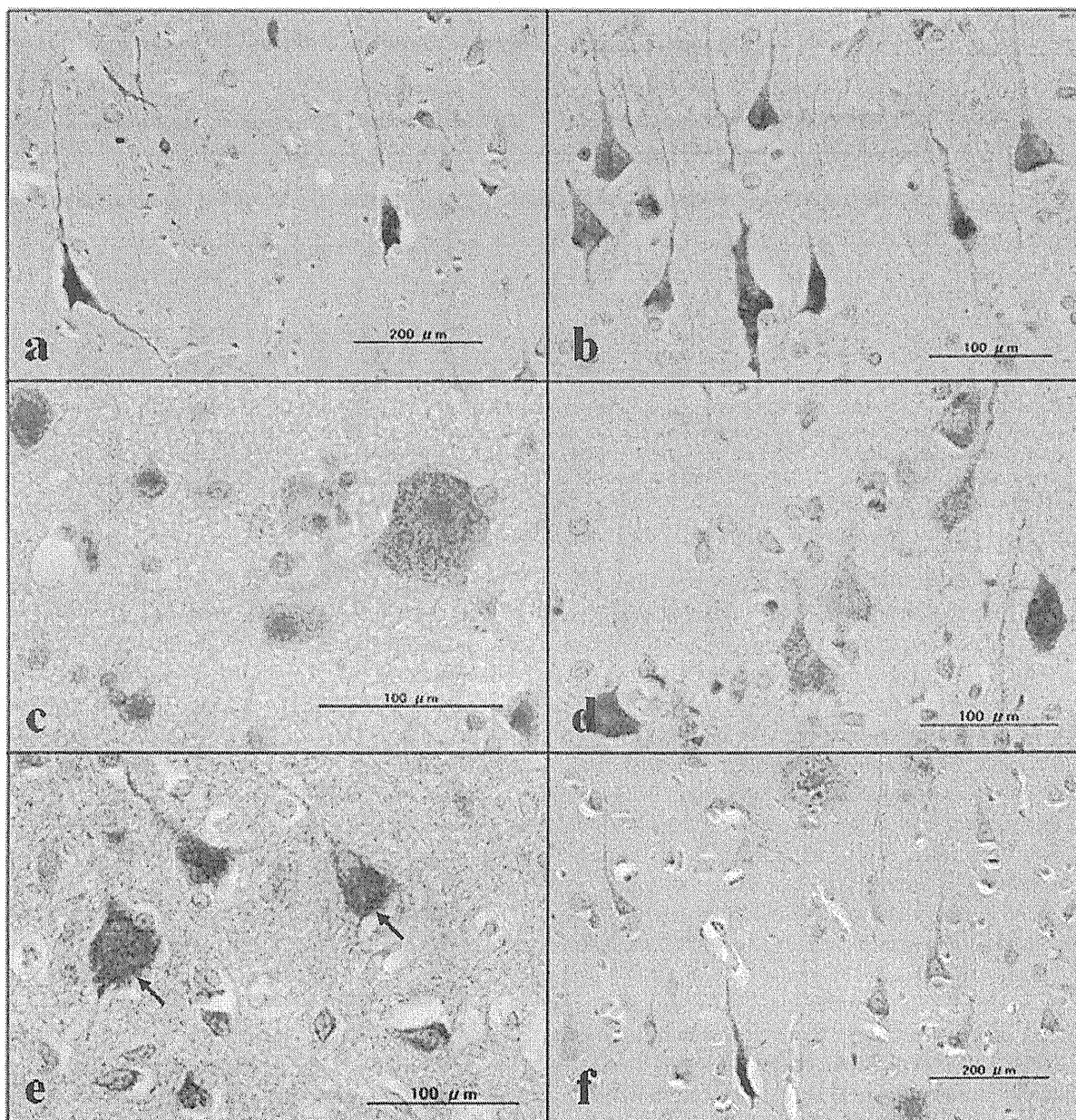


Figure 5. Neurone navigator 3 (NAV3) immunohistochemistry of the brains of neurodegenerative diseases. The expression of NAV3, paired helical filament (PHF)-tau and A β was studied in the frontal cortex tissue sections of Alzheimer disease (AD), amyotrophic lateral sclerosis (ALS) and Parkinson disease (PD) by immunohistochemistry. The panels (a–f) represent (a) NAV3 in AD-case 3, (b) NAV3 in AD-case 1, (c) NAV3 in ALS-case 4, (d) NAV3 in PD-case 3, (e) NAV3 (brown) and PHF-tau (red) double immunolabelling of AD-case 1 where the coexpression is indicated by arrows, and (f) NAV3 (brown) and A β (red) double immunolabelling of AD-case 3. In all the cases, large- and medium-sized pyramidal neurones in layers III and V express strong NAV3 immunoreactivity located in the cytoplasm, axons and dendrites. Notably, NAV3 immunoreactivity is the most intense in neurones with degenerating morphology bearing pyknotic nuclei in AD brains as shown in panels (a, b, f).

constitutively expressed at the outer nuclear membrane of neurones, and it is induced in reactive astrocytes after brain injury [20]. In contrast, we did not detect NAV3 immunoreactivity in reactive astrocytes in the brains of AD, PD and ALS. At present, it remains unknown whether enhanced expression of NAV3 in a subpopulation of cortical pyramidal neurones in AD brains reflects some pathogenetic changes or it is attributable to a compensatory mechanism against neurodegenerative events. By miRNA target database search, we found that not only miR-29, but also miR-19, miR-34 and miR-449, potentially down-regulate NAV3 expression (unpublished data), suggesting that multiple miRNAs converge on the regulation of NAV3 expression. Overall, the results of the present study could propose a possible scenario that underexpression of miR-29a affects neurodegenerative processes by up-regulating NAV3 and other miR-29a targets in AD brains. Further studies using large cohorts are required to clarify an active involvement of the miR-29a and NAV3 circuit in progression of neurodegeneration in AD.

Acknowledgements

Human brain tissues were provided by Research Resource Network, Japan. This work was supported by a research grant to J-IS from the High-Tech Research Center Project, the Ministry of Education, Culture, Sports, Science and Technology, Japan (S0801043) and a grant from Research on Intractable Diseases, the Ministry of Health, Labour and Welfare of Japan.

References

- 1 Kosik KS. The neuronal microRNA system. *Nat Rev Neurosci* 2006; 7: 911–20
- 2 Filipowicz W, Bhattacharyya SN, Sonenberg N. Mechanisms of post-transcriptional regulation by microRNAs: are the answers in sight? *Nat Rev Genet* 2008; 9: 102–14
- 3 Selbach M, Schwanhäusser B, Thierfelder N, Fang Z, Khanin R, Rajewsky N. Widespread changes in protein synthesis induced by microRNAs. *Nature* 2008; 455: 58–63
- 4 Fineberg SK, Kosik KS, Davidson BL. MicroRNAs potentiate neural development. *Neuron* 2009; 64: 303–9
- 5 Schratz GM, Tuebing F, Nigh EA, Kane CG, Sabatini ME, Kiebler M, Greenberg ME. A brain-specific microRNA regulates dendritic spine development. *Nature* 2006; 439: 283–9
- 6 Mellios N, Huang HS, Grigorenko A, Rogaev E, Akbarian S. A set of differentially expressed miRNAs, including miR-30a-5p, act as post-transcriptional inhibitors of BDNF in prefrontal cortex. *Hum Mol Genet* 2008; 17: 3030–42
- 7 Nelson PT, Wang WX, Rajeev BW. MicroRNAs (miRNAs) in neurodegenerative diseases. *Brain Pathol* 2008; 18: 130–8
- 8 Kim J, Inoue K, Ishii J, Vanti WB, Voronov SV, Murchison E, Hannon G, Abeliovich A. A MicroRNA feedback circuit in midbrain dopamine neurons. *Science* 2007; 317: 1220–4
- 9 Wang WX, Rajeev BW, Stromberg AJ, Ren N, Tang G, Huang Q, Rigoutsos I, Nelson PT. The expression of microRNA miR-107 decreases early in Alzheimer's disease and may accelerate disease progression through regulation of beta-site amyloid precursor protein-cleaving enzyme 1. *J Neurosci* 2008; 28: 1213–23
- 10 Hébert SS, Horré K, Nicolai L, Papadopoulou AS, Mandemakers W, Silaharoglu AN, Kauppinen S, Delacourte A, De Strooper B. Loss of microRNA cluster miR-29a/b-1 in sporadic Alzheimer's disease correlates with increased BACE1/beta-secretase expression. *Proc Natl Acad Sci USA* 2008; 105: 6415–20
- 11 Boissonneault V, Plante I, Rivest S, Provost P. MicroRNA-298 and microRNA-328 regulate expression of mouse β -amyloid precursor protein-converting enzyme 1. *J Biol Chem* 2009; 284: 1971–81
- 12 Hébert SS, Horré K, Nicolai L, Bergmans B, Papadopoulou AS, Delacourte A, De Strooper B. MicroRNA regulation of Alzheimer's amyloid precursor protein expression. *Neurobiol Dis* 2009; 33: 422–8
- 13 Lukiw WJ, Zhao Y, Cui JG. An NF- κ B-sensitive microRNA-146a-mediated inflammatory circuit in Alzheimer disease and in stressed human brain cells. *J Biol Chem* 2008; 283: 31315–22
- 14 Kocerha J, Kauppinen S, Wahlestedt C. microRNAs in CNS Disorders. *Neuromolecular Med* 2009; 11: 162–72
- 15 Mirra SS, Heyman A, McKeel D, Sumi SM, Crain BJ, Brownlee LM, Vogel FS, Hughes JP, van Belle G, Berg L. The Consortium to Establish a Registry for Alzheimer's Disease (CERAD). Part II. Standardization of the neuropathologic assessment of Alzheimer's disease. *Neurology* 1991; 41: 479–86
- 16 Braak H, Alafuzoff I, Arzberger T, Kretzschmar H, Del Tredici K. Staging of Alzheimer disease-associated neurofibrillary pathology using paraffin sections and immunocytochemistry. *Acta Neuropathol* 2006; 112: 389–404
- 17 Sethi P, Lukiw WJ. Micro-RNA abundance and stability in human brain: specific alterations in Alzheimer's disease temporal lobe neocortex. *Neurosci Lett* 2009; 459: 100–4
- 18 Mendes ND, Freitas AT, Sagot MF. Current tools for the identification of miRNA genes and their targets. *Nucleic Acids Res* 2009; 37: 2419–33
- 19 Kim J, Krichevsky A, Grad Y, Hayes GD, Kosik KS, Church GM, Ruvkun G. Identification of many microRNAs that

- copurify with polyribosomes in mammalian neurons. *Proc Natl Acad Sci USA* 2004; **101**: 360–5
- 20 Coy JF, Wiemann S, Bechmann I, Bächner D, Nitsch R, Kretz O, Christiansen H, Poustka A. Pore membrane and/or filament interacting like protein 1 (POMFIL1) is predominantly expressed in the nervous system and encodes different protein isoforms. *Gene* 2002; **290**: 73–94
 - 21 Aschrafi A, Schwlechter AD, Mameza MG, Natera-Naranjo O, Gioio AE, Kaplan BB. MicroRNA-338 regulates local cytochrome c oxidase IV mRNA levels and oxidative phosphorylation in the axons of sympathetic neurons. *J Neurosci* 2008; **28**: 12581–90
 - 22 Barik S. An intronic microRNA silences genes that are functionally antagonistic to its host gene. *Nucleic Acids Res* 2008; **36**: 5232–41
 - 23 van Rooij E, Sutherland LB, Thatcher JE, DiMaio JM, Naseem RH, Marshall WS, Hill JA, Olson EN. Dysregulation of microRNAs after myocardial infarction reveals a role of miR-29 in cardiac fibrosis. *Proc Natl Acad Sci USA* 2008; **105**: 13027–32
 - 24 Kapinas K, Kessler CB, Delany AM. miR-29 suppression of osteonectin in osteoblasts: regulation during differentiation and by canonical Wnt signaling. *J Cell Biochem* 2009; **108**: 216–24
 - 25 Fabbri M, Garzon R, Cimmino A, Liu Z, Zaneni N, Callegari E, Liu S, Alder H, Costinean S, Fernandez-Cymering C, Volinia S, Guler G, Morrison CD, Chan KK, Marcucci G, Calin GA, Huebner K, Croce CM. MicroRNA-29 family reverts aberrant methylation in lung cancer by targeting DNA methyltransferases 3A and 3B. *Proc Natl Acad Sci USA* 2007; **104**: 15805–10
 - 26 Mott JL, Kobayashi S, Bronk SF, Gores GJ. miR-29 regulates Mcl-1 protein expression and apoptosis. *Oncogene* 2007; **26**: 6133–40
 - 27 Xu H, Cheung IY, Guo HF, Cheung NK. MicroRNA miR-29 modulates expression of immunoinhibitory molecule B7-H3: potential implications for immune based therapy of human solid tumors. *Cancer Res* 2009; **69**: 6275–81
 - 28 Chang TC, Yu D, Lee YS, Wentzel EA, Arking DE, West KM, Dang CV, Thomas-Tikhonenko A, Mendell JT. Widespread microRNA repression by Myc contributes to tumorigenesis. *Nat Genet* 2008; **40**: 43–50
 - 29 Park SY, Lee JH, Ha M, Nam JW, Kim VN. miR-29 miRNAs activate p53 by targeting p85 alpha and CDC42. *Nat Struct Mol Biol* 2009; **16**: 23–9
 - 30 Wang H, Garzon R, Sun H, Ladner KJ, Singh R, Dahlman J, Cheng A, Hall BM, Qualman SJ, Chandler DS, Croce CM, Guttridge DC. NF-kappaB-YY1-miR-29 regulatory circuitry in skeletal myogenesis and rhabdomyosarcoma. *Cancer Cell* 2008; **14**: 369–81
 - 31 Gebeshuber CA, Zatloukal K, Martinez J. miR-29a suppresses tristetrarprolin, which is a regulator of epithelial polarity and metastasis. *EMBO Rep* 2009; **10**: 400–5
 - 32 Maes T, Barceló A, Buesa C. Neuron navigator: a human gene family with homology to *unc-53*, a cell guidance gene from *Caenorhabditis elegans*. *Genomics* 2002; **80**: 21–30
 - 33 Hekimi S, Kershaw D. Axonal guidance defects in a *Caenorhabditis elegans* mutant reveal cell-extrinsic determinants of neuronal morphology. *J Neurosci* 1993; **13**: 4254–71
 - 34 Muley PD, McNeill EM, Marzinke MA, Knobel KM, Barr MM, Clagett-Dame M. The atRA-responsive gene neuron navigator 2 functions in neurite outgrowth and axonal elongation. *Dev Neurobiol* 2008; **68**: 1441–53
 - 35 Karenko L, Hahtola S, Päivinen S, Karhu R, Syrjä S, Kähkönen M, Nedoszytko B, Kytölä S, Zhou Y, Blazevic V, Pesonen M, Nevala H, Nupponen N, Sihto H, Krebs I, Poustka A, Roszkiewicz J, Saksela K, Peterson P, Visakorpi T, Ranki A. Primary cutaneous T-cell lymphomas show a deletion or translocation affecting *NAV3*, the human *UNC-53* homologue. *Cancer Res* 2005; **65**: 8101–10
 - 36 Laloo B, Simon D, Veilla V, Lauzel D, Guyonnet-Duperat V, Moreau-Gaudry F, Sagliocco F, Grosset C. Analysis of post-transcriptional regulations by a functional, integrated, and quantitative method. *Mol Cell Proteomics* 2009; **8**: 1777–88

Supporting information

Additional Supporting Information may be found in the online version of this article:

Table S1. Characteristics of the study population.

Table S2. MicroRNA expression profiling of the frontal cortex of three ALS patients on a human miRNA microarray.

Table S3. Real-time RT-PCR analysis of miR-29a expression in the frontal cortex of human neurodegenerative diseases.

Please note: Wiley-Blackwell are not responsible for the content or functionality of any supporting materials supplied by the authors. Any queries (other than missing material) should be directed to the corresponding author for the article.

Received 18 December 2009

Accepted after revision 1 February 2010

Published online Article Accepted on 25 February 2010

BmDJ-1 Is a Key Regulator of Oxidative Modification in the Development of the Silkworm, *Bombyx mori*

Hiroko Tabunoki^{1*}, Hiroaki Ode¹, Yutaka Banno², Susumu Katsuma³, Toru Shimada³, Kazuei Mita⁴, Kimiko Yamamoto⁴, Ryoichi Sato⁵, Reiko Ishii-Nozawa⁶, Jun-ichi Satoh¹

1 Department of Bioinformatics and Molecular Neuropathology, Meiji Pharmaceutical University, Tokyo, Japan, **2** The Center of Genetic Resources, University of Kyushu, Fukuoka, Japan, **3** Department of Agricultural and Environmental Biology, Graduate School of Agricultural and Life Sciences, The University of Tokyo, Tokyo, Japan, **4** Insect Genome Laboratory, National Institute of Agrobiological Sciences, Tsukuba, Japan, **5** Bio-Applications and Systems Engineering, Tokyo University of Agriculture and Technology, Koganei, Tokyo, Japan, **6** Department of Clinical Pharmacology, Meiji Pharmaceutical University, Tokyo, Japan

Abstract

We cloned cDNA for the *Bombyx mori* DJ-1 protein (BmDJ-1) from the brains of larvae. BmDJ-1 is composed of 190 amino acids and encoded by 672 nucleotides. Northern blot analysis showed that BmDJ-1 is transcribed as a 756-bp mRNA and has one isoform. Reverse transcriptase (RT)-PCR experiments revealed that the BmDJ-1 was present in the brain, fatbody, Malpighian tubule, ovary and testis but present in only low amounts in the silkgland and hemocyte of day 4 fifth instar larvae. Immunological analysis demonstrated the presence of BmDJ-1 in the brain, midgut, fatbody, Malpighian tubule, testis and ovary from the larvae to the adult. We found that BmDJ-1 has a unique expression pattern through the fifth instar larval to adult developmental stage. We assessed the anti-oxidative function of BmDJ-1 using rotenone (ROT) in day 3 fifth instar larvae. Administration of ROT to day 3 fifth instar larvae, together with exogenous (BmNPV-BmDJ-1 infection for 4 days in advance) BmDJ-1, produced significantly lower 24-h mortality in BmDJ-1 groups than in the control. 2D-PAGE revealed an isoelectric point (pI) shift to an acidic form for BmDJ-1 in BmN4 cells upon ROT stimulus. Among the factors examined for their effects on expression level of BmDJ-1 in the hemolymph, nitric oxide (NO) concentration was identified based on dramatic developmental stage-dependent changes. Administration of isosorbide dinitrate (ISDN), which is an NO donor, to BmN4 cells produced increased expression of BmDJ-1 compared to the control. These results suggest that BmDJ-1 might control oxidative stress in the cell due to NO and serves as a development modulation factor in *B. mori*.

Citation: Tabunoki H, Ode H, Banno Y, Katsuma S, Shimada T, et al. (2011) BmDJ-1 Is a Key Regulator of Oxidative Modification in the Development of the Silkworm, *Bombyx mori*. PLoS ONE 6(3): e17683. doi:10.1371/journal.pone.0017683

Editor: Bob Lightowers, Newcastle University, United Kingdom

Received: October 22, 2010; **Accepted:** February 8, 2011; **Published:** March 24, 2011

Copyright: © 2011 Tabunoki et al. This is an open-access article distributed under the terms of the Creative Commons Attribution License, which permits unrestricted use, distribution, and reproduction in any medium, provided the original author and source are credited.

Funding: H.T. was supported by the Ministry of Education, Science, Sports and Culture, Grant-in-Aid (<http://www.jsps.go.jp/english/e-grants/grants.html>) for Young Scientists (B), 2010, 22710195. This work was in part supported by grants from the High-Tech Research Center Project (<http://www.mext.go.jp/english/>), the Ministry of Education, Culture, Sports, Science and Technology (MEXT), Japan (S0801043), and the Research on Intractable Diseases (<http://www.nanbyou.or.jp/english/index.htm>), the Ministry of Health, Labour and Welfare of Japan (H22-Nanchi-Ippan-136) to J.S. The funders had no role in study design, data collection and analysis, decision to publish, or preparation of the manuscript. There was no additional external funding received for this study.

Competing Interests: The authors have declared that no competing interests exist.

* E-mail: tabunoki@my-pharm.ac.jp

Introduction

The protein DJ-1 is ubiquitously expressed in cells and it is highly conserved across a wide variety of organisms, showing moderate sequence identity with heat shock protein 31 (HSP31) chaperones and ThiJ/PfpI cysteine proteases [1]. Mutated forms of DJ-1 are known to cause early onset autosomal recessive juvenile Parkinson's disease (PD), and many studies have demonstrated a neuro-protective role of DJ-1. DJ-1, which is encoded by PARK7, is a multi-functional protein that plays roles in chaperoning, RNA-binding, SUMOylation, apoptosis, and protease activity [2].

Additionally, DJ-1 is induced by oxidative modification and is rapidly oxidized at position Cys 106 [3]. Oxidative modification leads to mitochondrial damage in cultured cells exposed to 1-methyl-4-phenyl-1,2,3,6 tetrahydropyridine (MPTP), 6-hydroxydopamine (6-OHDA), paraquat (PQ), and rotenone (ROT), which inhibit the mitochondrial electron transfer chain of mitochondrial complex I [4]. These compounds enhance production of reactive oxygen species (ROS) and reduce production of ATP, resulting in

mitochondria dysfunction [5]. DJ-1 seems to directly scavenge free radicals from mitochondria in response to these oxidative stresses. MPTP, 6-OHDA, PQ, and ROT are used to produce PD models in rats and *Drosophila* and to analyze the pathology of PD [6,7].

DJ-1 has a dimer structure, and the L166P mutation produces structural perturbation that causes the protein to be ubiquitinated and susceptible to degradation by the 26S proteasome, significantly reducing its half-life *in vivo* [8,9]. L166P DJ-1 forms unstable dimers with disrupted protein folding and function [10]. The G106A mutation results in a loss-of-function of DJ-1 protease and chaperone activity [11,12]. However, the precise pathology due to mutations and species-specific biological functions of DJ-1 remain unclear.

The silkworm, *Bombyx mori*, a Lepidopteran insect, has been utilized as a model system for basic science research because of its well-characterized genome, availability of various genetic mutants, and the development of transgenic, RNAi, and microarray technologies [13,14,15,16,17]. The complete silkworm genome has approximately 18,510 genes, including a substantial number of mammalian orthologs [13,16].

In the present study, we cloned the silkworm *B. mori* DJ-1 ortholog (BmDJ-1), clarified its expression pattern during development, and examined its anti-oxidative function. BmDJ-1 is a newly identified member of the DJ-1 family and is a growth-associated protein that is altered with development in *B. mori*.

Results

Molecular cloning of BmDJ-1

Amplifying BmDJ-1 by RT-PCR with 5' RACE using gene-specific primers from *B. mori* larvae brain cDNA produced an 86-bp product. The Kozak consensus sequence AAAATGAAG [18] was found to be present at the site of translation initiation determined using NetStart software [19]. Therefore, we determined that the cDNA encoded a putative 5'-untranslated sequence of 95 bp, an ATG start site, and an open reading frame (ORF) at position 96 extending to position 668. The deduced ORF of BmDJ-1 was composed of 672 nucleotides comprising 190 amino acids, had a molecular weight of 20,113 Dalton, and a putative isoelectric point (pI) of 5.15.

The nucleotide sequence reported in this paper has been submitted to GeneBank/DBJ SAKURA Data bank Accession No. AB281053.

A computer search of the SMART database (<http://smart.embl-heidelberg.de/>) revealed that BmDJ-1 contained a DJ-1_PfpI domain at position 31T-173T. We identified the location of the BmDJ-1 gene in scaffold 2995719-2998746 of chromosome 23 at the splitting of 5 blocks by linkage mapping 28 chromosomes by SNP markers [20].

A BLAST search showed that BmDJ-1 has 50% amino acid sequence identity to *D. rerio* DJ-1 (NCBI gene ID:449674) and *D. melanogaster* DJ-1 beta (NCBI gene ID:43652); 47% amino acid sequence identity to *H. sapiens* (NCBI gene ID:11315), *X. tropicalis* (NCBI gene ID:548568), *G. gallus* (NCBI gene ID:395227), *B. taurus* (NCBI gene ID:511268), and *R. novaltis* (NCBI gene ID:117287) DJ-1; 46% amino acid sequence identity to *C. elegans* (NCBI gene ID:183625) and *M. musculus* (NCBI gene ID:57320) DJ-1; and 45% amino acid sequence identity to *D. melanogaster* DJ-1 alpha (NCBI gene ID:36543). An alignment of the deduced BmDJ-1 amino acid sequences and DJ-1 orthologs from other species using CLC Work Bench 3.2.3 showed that the BmDJ-1 protein sequence contains all of the conserved Cys and Leu residues (Fig. 1-A, black asterisks).

The phylogenetic tree placed *D. melanogaster* DJ-1 and BmDJ-1 into a distinct cluster (Fig. 1-B).

BmDJ-1 mRNA is expressed in various tissues in fifth instar larvae

Northern blot analysis revealed that there is a single transcription product for BmDJ-1 with a size of 756 bp (Fig. 2A).

We used RT-PCR to investigate the expression profile of BmDJ-1 mRNA in various tissues. BmDJ-1 showed high expression in the brain, fatbody, Malpighian tubule, ovary, and testis (Fig. 2B, upper panel lanes 2, 5–8) and low expression in the midgut, silk gland, and hemocyte (Fig. 2B, upper panel lanes 3, 4, 9).

Specificity of antibody against BmDJ-1

We examined the utility of anti-BmDJ-1 antibodies raised against the recombinant Xpress-tagged BmDJ-1 to identify BmDJ-1. Anti-BmDJ-1 antibody reacted with both recombinant BmDJ-1 protein as a 25-KDa band and BmDJ-1 in the cell and tissue lysate from *B. mori* as a 20-KDa band. In contrast, BmDJ-1 antibodies did not recognize recombinant carotenoid binding protein (CBP)

from *B. mori* tagged with GST [21] and HEK 293 cell lysate (Fig. 3, lanes 1 and 4). The molecular weight of the recombinant BmDJ-1 protein (Fig. 3, lanes 2 and 3) was slightly greater than the endogenous BmDJ-1 protein (Fig. 3, lanes 5 and 6), excluding the possibility of non-specific binding to the Xpress tag.

Identification of developmental stage and tissue-specific expression patterns of BmDJ-1 by immunoblotting

Distribution of BmDJ-1 expression by developmental stage and tissue is shown in Figure 4. Whole body expression is roughly equal for all larval instars, pupae, and adults (Fig. 4A and S1A, lanes 1–7). Moreover, equal amounts of BmDJ-1 are found in the brains of fifth instar larvae, pupae, and adults, but it is slightly increased in larvae (Fig. 4B and S1B, lanes 8–10). To determine the distribution pattern of BmDJ-1, we studied tissues (midgut, fatbody, Malpighian tubule, ovary, and testis; Fig. 4C and S1C) from day 0 fifth instar larvae to adults by immunoblotting. BmDJ-1 was expressed in the larval through adult developmental stages in these tissues, but expression was low in day 1 pupae (fatbody, Malpighian tubule and ovary; Fig. 4C, panels b, c, e, lane 14). Expression levels increased with pupal stadium from day 0 to 4 (Fig. 4C, panels f–h) and high levels of BmDJ-1 expression were also identified in the testis during these developmental stages (Fig. 4C, panel j). Therefore, BmDJ-1 showed a unique day-to-day expression pattern from day 0 fifth instar larvae to the adult developmental stages.

The pI of BmDJ-1 shifted acidic by ROT stimulation

Treatment of BmN4 cells with 50 μ M ROT produced a shift in the pI to acidic, as shown on 2D-PAGE and immunoblotting (Fig. 5).

BmDJ-1 overexpression in larvae causes resistance to ROT

ROT was used to produce an oxidative stress in order to examine the effect of exogenous BmDJ-1 protein. We determined the lethal dose (LD) of ROT for day 3 fifth instar larvae of 10.1 μ g/g (LD₅₀; 95% CI, 6.02–17.4) (Fig. 6). Based on computer simulations of reactivity using SAS software, we determined the optimal ROT concentration for further testing of the protective effects of BmDJ-1 to be 20 μ g/g.

A BmDJ-1 overexpressing silkworm produced by injecting day 0 fifth instar larvae with recombinant BmNPV-BmDJ-1 virus showed significantly decreased mortality following intrahemocoelomic injection of 20 μ g/g ROT after 4 days (day 3 fifth instar larvae). For three experiments, the BmDJ-1 group mortality of 38, 27, and 15% was significantly lower than mortality rates of the blank vectors (control) of 81, 93, and 90%, respectively ($P < 0.01$, < 0.001 , < 0.001 , respectively; Table 1).

We also confirmed virus-derived BmDJ-1 expression levels in the fatbodies of several insects after 1 day (24 h) and 4 days (day 4 fifth instar larvae) by RT-PCR and after 4 days by immunoblotting. Expression of blank-vector recombinant virus was detected as a 300-bp band, while virus-derived BmDJ-1 expression was detected as an 850-bp band. The BmDJ-1 expression was absent at 24 h but was detected at 96 h (Fig. 7A). Virus-derived BmDJ-1 protein was expressed at about 2-fold greater levels in non-infected groups after 4 days, and BmDJ-1 protein expression in blank virus-infected control groups was significantly decreased (Fig. 7B and S2).

Expression of BmDJ-1 and NO concentration

The expression pattern of BmDJ-1 was tissue-specific, reflecting the unique responses to oxidative stress. We examined some

A

		70		80	
<i>B.mori</i>	M	-----	-----	-----	KGAEVLEIA - Q 11
<i>H.sapiens</i>	MA	-----	-----	-----	KRAEMLEIA - K 12
<i>B.taurus</i>	MA	-----	-----	-----	KRAEMLEIA - K 12
<i>M.musculus</i>	MA	-----	-----	-----	KRAEMLEIA - K 12
<i>G.gallus</i>	MA	-----	-----	-----	KRAEMLEIA - K 12
<i>D.ferio</i>	M	-----	-----	-----	KRAEMLEIA - K 12
<i>X.tropicalis</i>	MA	-----	-----	-----	KRAEMLEIA - K 12
<i>A.aegypti</i>	M	-----	-----	-----	KRAEMLEIA - K 11
<i>C.elegans</i>	MA	-----	-----	-----	KRAEMLEIA - K 13
<i>D.melanogaster-beta</i>	M	-----	-----	-----	KRAEMLEIA - P 20
<i>D.melanogaster-alpha</i>	M	-----	-----	-----	KRAEMLEIA - P 20
<i>Consensus</i>	MA	-----	-----	-----	KRALVLEIA - K
Conservation					
		90		100	
<i>B.mori</i>	GA	EMETVIFP	VDMNRKAGIK	VTVAQLAGKE	FVQCSRDVVI 51
<i>H.sapiens</i>	GA	EMETVIFP	VDMNRKAGIK	VTVAQLAGKE	FVQCSRDVVI 52
<i>B.taurus</i>	GA	EMETVIFP	VDMNRKAGIK	VTVAQLAGKE	FVQCSRDVVI 52
<i>M.musculus</i>	GA	EMETVIFP	VDMNRKAGIK	VTVAQLAGKE	FVQCSRDVVI 52
<i>G.gallus</i>	GA	EMETVIFP	VDMNRKAGIK	VTVAQLAGKE	FVQCSRDVVI 52
<i>D.ferio</i>	GA	EMETVIFP	VDMNRKAGIK	VTVAQLAGKE	FVQCSRDVVI 52
<i>X.tropicalis</i>	GA	EMETVIFP	VDMNRKAGIK	VTVAQLAGKE	FVQCSRDVVI 52
<i>A.aegypti</i>	GA	EMETVIFP	VDMNRKAGIK	VTVAQLAGKE	FVQCSRDVVI 50
<i>C.elegans</i>	GA	EMETVIFP	VDMNRKAGIK	VTVAQLAGKE	FVQCSRDVVI 53
<i>D.melanogaster-beta</i>	GA	EMETVIFP	VDMNRKAGIK	VTVAQLAGKE	FVQCSRDVVI 53
<i>D.melanogaster-alpha</i>	GA	EMETVIFP	VDMNRKAGIK	VTVAQLAGKE	FVQCSRDVVI 53
<i>Consensus</i>	GA	EMETVIFP	VDMNRKAGIK	VTVAQLAGKE	FVQCSRDVVI
Conservation					
		110		120	
<i>B.mori</i>	CP	PTSLICPAIK	KEGPDYDVMV	LRGGLLGCAN	AGEEAAYKIV 91
<i>H.sapiens</i>	CP	PTSLICPAIK	KEGPDYDVMV	LRGGLLGCAN	AGEEAAYKIV 91
<i>B.taurus</i>	CP	PTSLICPAIK	KEGPDYDVMV	LRGGLLGCAN	AGEEAAYKIV 91
<i>M.musculus</i>	CP	PTSLICPAIK	KEGPDYDVMV	LRGGLLGCAN	AGEEAAYKIV 91
<i>G.gallus</i>	CP	PTSLICPAIK	KEGPDYDVMV	LRGGLLGCAN	AGEEAAYKIV 91
<i>D.ferio</i>	CP	PTSLICPAIK	KEGPDYDVMV	LRGGLLGCAN	AGEEAAYKIV 91
<i>X.tropicalis</i>	CP	PTSLICPAIK	KEGPDYDVMV	LRGGLLGCAN	AGEEAAYKIV 91
<i>A.aegypti</i>	CP	PTSLICPAIK	KEGPDYDVMV	LRGGLLGCAN	AGEEAAYKIV 91
<i>C.elegans</i>	CP	PTSLICPAIK	KEGPDYDVMV	LRGGLLGCAN	AGEEAAYKIV 107
<i>D.melanogaster-beta</i>	CP	PTSLICPAIK	KEGPDYDVMV	LRGGLLGCAN	AGEEAAYKIV 110
<i>D.melanogaster-alpha</i>	CP	PTSLICPAIK	KEGPDYDVMV	LRGGLLGCAN	AGEEAAYKIV 110
<i>Consensus</i>	CP	PTSLICPAIK	KEGPDYDVMV	LRGGLLGCAN	AGEEAAYKIV
Conservation					
		140		150	
<i>B.mori</i>	KA	AECAAPITM	IAKHGVAQCK	VEITDHPMKP 126	
<i>H.sapiens</i>	KA	AECAAPITM	IAKHGVAQCK	VEITDHPMKP 126	
<i>B.taurus</i>	KA	AECAAPITM	IAKHGVAQCK	VEITDHPMKP 126	
<i>M.musculus</i>	KA	AECAAPITM	IAKHGVAQCK	VEITDHPMKP 126	
<i>G.gallus</i>	KA	AECAAPITM	IAKHGVAQCK	VEITDHPMKP 126	
<i>D.ferio</i>	KA	AECAAPITM	IAKHGVAQCK	VEITDHPMKP 126	
<i>X.tropicalis</i>	KA	AECAAPITM	IAKHGVAQCK	VEITDHPMKP 126	
<i>A.aegypti</i>	KA	AECAAPITM	IAKHGVAQCK	VEITDHPMKP 126	
<i>C.elegans</i>	KA	AECAAPITM	IAKHGVAQCK	VEITDHPMKP 147	
<i>D.melanogaster-beta</i>	KA	AECAAPITM	IAKHGVAQCK	VEITDHPMKP 147	
<i>D.melanogaster-alpha</i>	KA	AECAAPITM	IAKHGVAQCK	VEITDHPMKP 147	
<i>Consensus</i>	KA	AECAAPITM	IAKHGVAQCK	VEITDHPMKP	
Conservation					
		170		200	
<i>B.mori</i>	KMMN	GDHYKY	SEDR	VVKDG	NIITSRGPGT 170
<i>H.sapiens</i>	KMMN	GDHYKY	SEDR	VVKDG	NIITSRGPGT 170
<i>B.taurus</i>	KMMN	GDHYKY	SEDR	VVKDG	NIITSRGPGT 170
<i>M.musculus</i>	KMMN	GDHYKY	SEDR	VVKDG	NIITSRGPGT 170
<i>G.gallus</i>	KMMN	GDHYKY	SEDR	VVKDG	NIITSRGPGT 170
<i>D.ferio</i>	KMMN	GDHYKY	SEDR	VVKDG	NIITSRGPGT 170
<i>X.tropicalis</i>	KMMN	GDHYKY	SEDR	VVKDG	NIITSRGPGT 170
<i>A.aegypti</i>	KMMN	GDHYKY	SEDR	VVKDG	NIITSRGPGT 166
<i>C.elegans</i>	KMMN	GDHYKY	SEDR	VVKDG	NIITSRGPGT 166
<i>D.melanogaster-beta</i>	KMMN	GDHYKY	SEDR	VVKDG	NIITSRGPGT 195
<i>D.melanogaster-alpha</i>	KMMN	GDHYKY	SEDR	VVKDG	NIITSRGPGT 195
<i>Consensus</i>	KMMN	GDHYKY	SEDR	VVKDG	NIITSRGPGT
Conservation					
		220		400	
<i>B.mori</i>	ALV	GKEVADQ	VKAP	LLL - K D 100	
<i>H.sapiens</i>	ALV	GKEVADQ	VKAP	LLL - K D 100	
<i>B.taurus</i>	ALV	GKEVADQ	VKAP	LLL - K D 100	
<i>M.musculus</i>	ALV	GKEVADQ	VKAP	LLL - K D 100	
<i>G.gallus</i>	ALV	GKEVADQ	VKAP	LLL - K D 100	
<i>D.ferio</i>	ALV	GKEVADQ	VKAP	LLL - K D 100	
<i>X.tropicalis</i>	ALV	GKEVADQ	VKAP	LLL - K D 100	
<i>A.aegypti</i>	ALV	GKEVADQ	VKAP	LLL - K D 100	
<i>C.elegans</i>	ALV	GKEVADQ	VKAP	LLL - K D 107	
<i>D.melanogaster-beta</i>	ALV	GKEVADQ	VKAP	LLL - K D 205	
<i>D.melanogaster-alpha</i>	ALV	GKEVADQ	VKAP	LLL - K D 217	
<i>Consensus</i>	ALV	GKEVADQ	VKAP	LLL - K D	
Conservation					

B

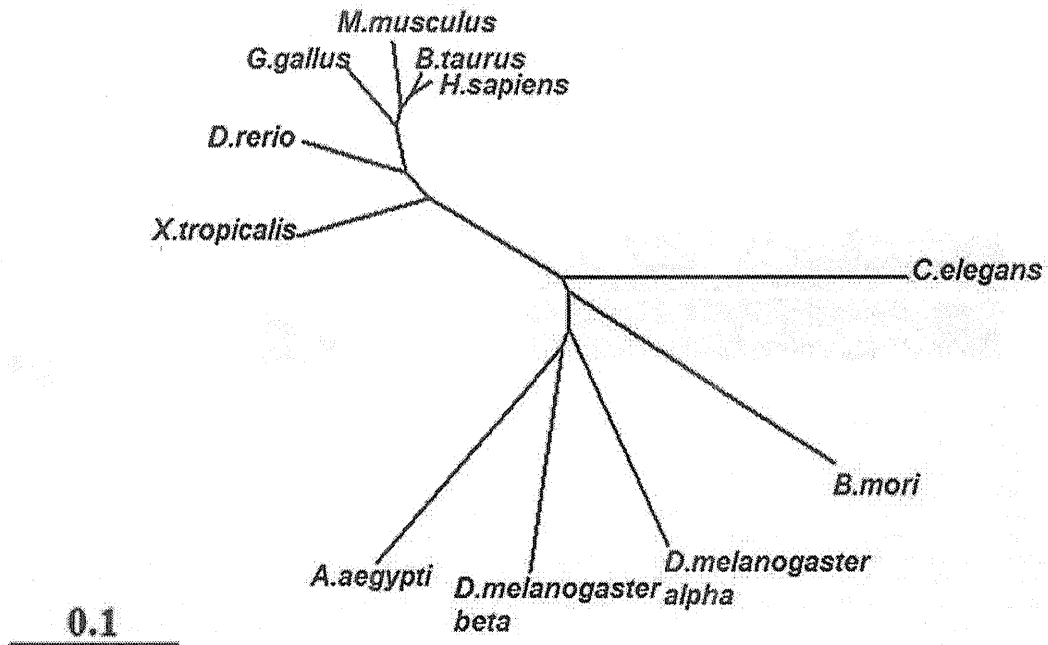


Figure 1. Alignment and Phylogenetic tree of *B. mori* DJ-1 with other DJ-1 proteins. A. Conserved amino acid sequences C at position 106 and L at position 166 of human DJ-1 are marked by asterisks (*). The level of conserved amino acid residues among the various species are graphically shown below the sequences. The residues of the alignment are color-coded according to the Rasmol color scheme (<http://life.nthu.edu.tw/fmhsu/rasframe/COLORS.HTM#aminocolors>) B. The unrooted bootstrap tree of *B. mori* DJ-1 and DJ-1 protein of other species. Sequences are *Homo sapiens*, *Bos Taurus*, *Mus musculus*, *Gallus gallus*, *Danio rerio*, *Xenopus tropicalis*, *Drosophila melanogaster*- α and - β , *Caenorhabditis elegans*, and *Bombyx mori* DJ-1. doi:10.1371/journal.pone.0017683.g001

factors that might affect expression. NO concentration in the hemolymph was found to fluctuate from the fifth instar larva to adult (Fig. 8A), with high levels for day 0 and 6 fifth instar larvae and adults and gradually increasing NO concentration in the pupal stages. To test whether NO affects the expression of BmDJ-1, BmN4 cells were treated with 100 μ M ISDN as an NO donor for 16 h. BmDJ-1 was detected in each sample by SDS-PAGE and immunoblotting with NO concentration (Fig. 8B) and BmDJ-1 expression (Fig. 8C and S3) increased compared to the control (0.1% ethanol).

Discussion

Throughout its evolutionary history, DJ-1 shows a highly conserved amino acid sequence. Characterization of the *B. mori* variant, BmDJ-1, by cDNA cloning from the brains of the fifth instar larvae shows the presence of Cys and Leu, which are key residues for the function of DJ-1.

On a phylogenetic tree of DJ-1 proteins, two orthologs of *D. melanogaster*, DJ-1 α and DJ-1 β , and BmDJ-1 placed in distinct

clusters. *D. melanogaster* DJ-1 α is most highly expressed in the testis from the pupal stages to adult, and DJ-1 β is expressed in almost all tissues from embryo to adult. Loss-of-function DJ-1 β mutant flies are sensitive to oxidative modification from H₂O₂ and paraquat, although the role played by DJ-1 α remains unclear [22]. Thus, these two *D. melanogaster* DJ-1s appear to have distinct functions.

In contrast, BmDJ-1 exists as a single isoform based on the single 756-bp transcript and only one band for BmDJ-1 on northern blot assay. The EST database (SilkBase; <http://morus.ab.a.u-tokyo.ac.jp/cgi-bin/index.cgi>) shows two distinct EST clones (data not shown). While BmDJ-1 may exist as several kinds of splice variants, this could not be clarified in this study.

BmDJ-1 demonstrated resistance to oxidative stress by ROT

DJ-1 has been reported to play a role in anti-oxidative stress by several independent groups. We confirmed that BmDJ-1 changes to an acidic form that is affected by ROT treatment in BmN4 cells (Fig. 5), indicating a response to oxidative stress.

In exogenous tests of BmDJ-1 with ROT, the mortality rate of individuals with BmDJ-1 is significantly decreased in the presence of ROT treatment, while the control groups remain extremely sensitive. It has been reported that the start of protein synthesis for BmNPV is 24 h after infection and that the protein expression level peaks at 96 h [23]. Endogenous protein synthesis stopped at 24 h. Immunoblotting at 96 h showed that virus-derived BmDJ-1 protein expression was significantly increased and virus-infection control group of BmDJ-1 protein expression was significantly decreased. Our findings of virus-derived BmDJ-1 expression after 96 h corroborate those results and suggest that BmDJ-1 overexpression improves the survival of silkworm larvae treated with ROT.

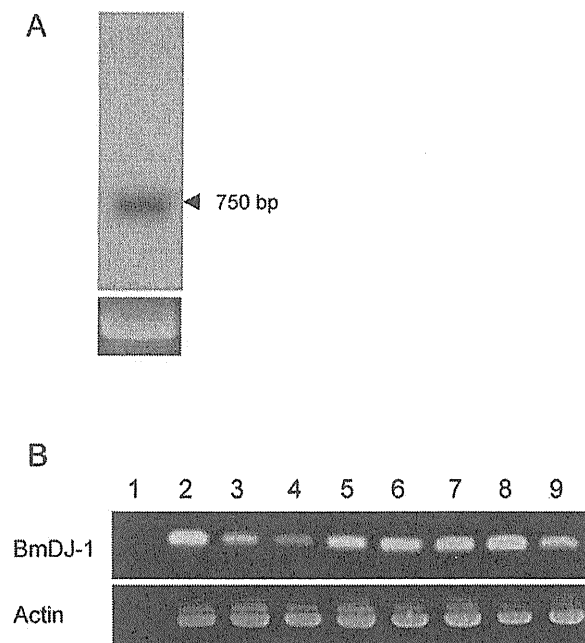


Figure 2. Northern blot analysis and RT-PCR of BmDJ-1. A. Total RNA isolated from *B. mori* ovary was analyzed by northern blot analysis using a BmDJ-1 probe. A band at about 756 bp was identified as the BmDJ-1 transcript. The amount of total RNA is 12 μ g per lane. 18S ribosomal RNA was used as a control for monitoring RNA loading. B. RT-PCR for BmDJ-1 from cDNA samples synthesized from diverse larval tissues. RT-PCR for actin was used as a positive loading control and RT-PCR reaction, without reverse transcriptase, was used as a negative control. Lane 1, brain (RT-); lane 2, brain; lane 3, midgut; lane 4, silk gland; lane 5, fat body; lane 6, Malpighian tubule; lane 7, ovary; lane 8, testis; lane 9, hemocyte. doi:10.1371/journal.pone.0017683.g002

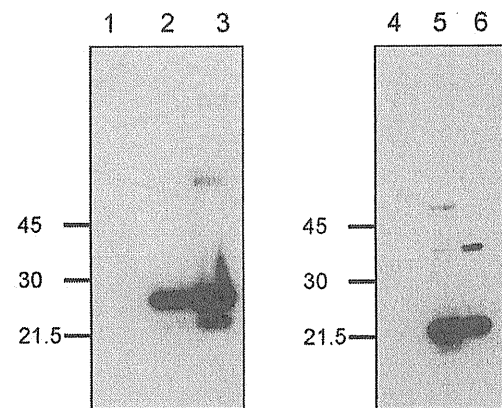


Figure 3. Specificity of anti-BmDJ-1 antibody. The recombinant protein, cell or tissue lysate were separated on a 12% SDS-PAGE gel, transferred onto a nitrocellulose membrane, and processed for immunoblotting with anti-BmDJ-1 antibody. The following samples were loaded in each lane: 1, 1 μ g recombinant CBP as a negative control; 2, 0.25 μ g recombinant BmDJ-1 protein; 3, 0.5 μ g recombinant BmDJ-1 protein; 4, HEK 293 cells; 5, BmN4 cells; 6, larvae brain. doi:10.1371/journal.pone.0017683.g003

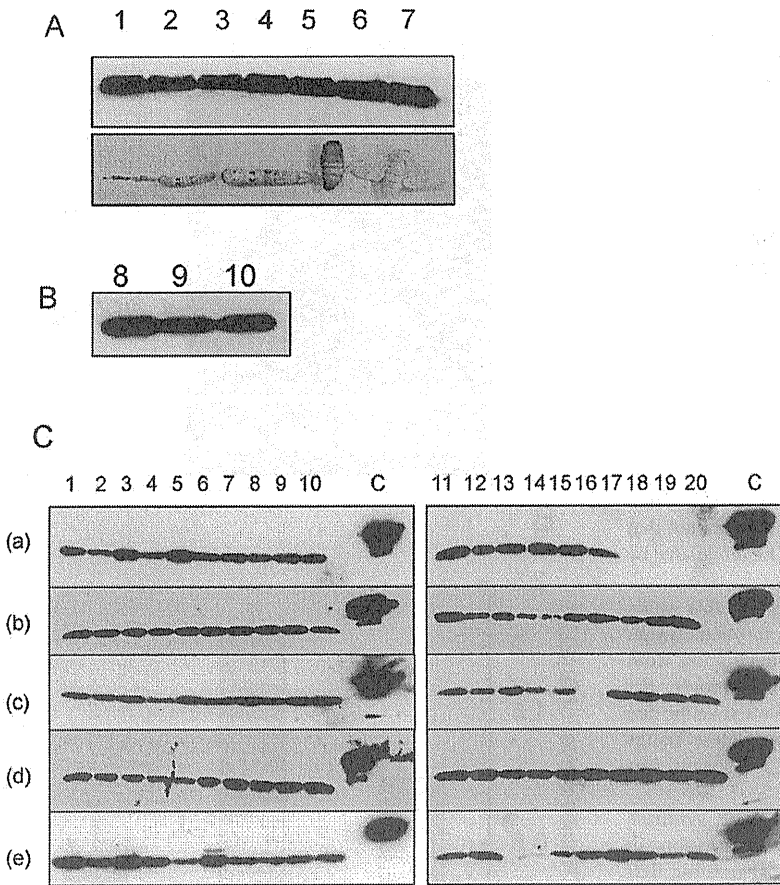


Figure 4. Developmental and tissue distribution of BmDJ-1 in *B. mori*. A. Aliquots (5 µg) of whole body homogenates from day 0 larvae of the first (lane 1), second (lane 2), third (lane 3), fourth (lane 4), and fifth (lane 5) instars, the pupae (lane 6), and the adult (lane 7) were separated by SDS-PAGE, transferred to nitrocellulose, and probed with anti-BmDJ-1 antibody. B. Aliquots (5 µg) of brain of the fifth instar larvae (lane 8), pupae (lane 9), and adults (lane 10). C. Aliquots (5 µg) of protein of various tissues were subjected to SDS-PAGE and examined for BmDJ-1 expression. The following tissues are shown: a, midgut; b, fatbody; c, Malpighian tubule; d, testis; and e, ovary were isolated from day 0 to 12 fifth instar larvae (lanes 1 to 13), from day 0, 1, 3, 4, 7 and 8 pupae (lanes 14 to 19), and from day 0 adults (lane 20). No samples were loaded in panel a, lanes 17, 18, 19, 20; panel c, lane 16; and panel e, lane 13.
doi:10.1371/journal.pone.0017683.g004

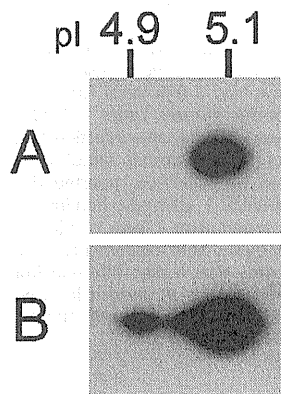


Figure 5. Effect of BmDJ-1 on ROT-induced oxidative stress in BmN4 cells. A. BmN4 cells exposed to ROT for 3 h were examined for BmDJ-1 content by 2D-PAGE and immunoblotting. A is control, B is ROT treatment.
doi:10.1371/journal.pone.0017683.g005

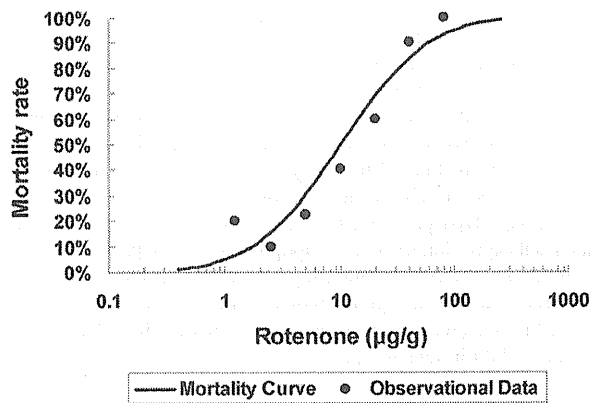


Figure 6. Dose mortality curve of rotenone in the silkworm. ROT (0, 1.25, 2.5, 5.0, 10, 20, 40, and 80 µg/g) was injected in day 3 fifth instar larvae, and the mortality rate within 24 h was examined. Filled circles were observational data.
doi:10.1371/journal.pone.0017683.g006

Table 1. Mortality rate of BmDJ-1 overexpressing (rBmNPV-infected) silkworm exposed to ROT oxidative stress.

Experiment	Silkworm mortality ^a (%)	
	Control	BmDJ-1
1	17/20 (85)	8/21 (38)**
2	14/15 (93)	4/15 (27)***
3	18/20 (90)	3/20 (15)***

^aRotenone (20 µg/g) was injected into BmDJ-1 overexpressing day 3 fifth instar larvae as shown in Fig. 7, and the mortality rate (dead silkworms/total silkworms; mortality rate, % in parentheses) within 24 h was examined.

**P<0.01.

***P<0.001 compared with control values.

doi:10.1371/journal.pone.0017683.t001

BmDJ-1 expression controlled with NO

BmDJ-1 showed a tissue-specific expression pattern that indicates unique responses to oxidative stress. We found that NO was an oxidative stressor in *B. mori* that could be modulated by BmDJ-1.

The BmDJ-1 expression pattern in tissues in this study suggested that BmDJ-1 expression correlates to the hemolymph NO concentration, which showed day-to-day fluctuation from fifth instar larvae to adult (Figs. 4C and 8A). Moreover, the expression of BmDJ-1 was increased and the pI shifted acidic due to exposure to an NO donor (data not shown). These results showed that BmDJ-1 was oxidized and its expression was regulated by NO.

Choi et al. [24] reported that the nitric oxide synthase (NOS) gene in *B. mori* shows the highest expression in Malpighian tubule in day 7 fifth instar larvae, suggesting that NO might be related to *B. mori* metamorphosis. Inoue et al. [25] reported that administration of ISDN, an NO donor, to the beetle *Homoderus mellyi parry* rapidly progresses pupation. Conversely, the administration of carnitine, which suppresses apoptosis of cells in larval beetles, extended the larval developmental period and generated huge adult beetles. These observations implicate NO in the mechanism of metamorphosis as an apoptosis initiator, though the underlying process remains unclear.

In *B. mori*, apoptosis is the principal mechanism for dynamic remodeling of the body structure during metamorphosis. Apoptosis mainly occurs during the pupal developmental period, during which the restructuring produces the adult body. In our observation, the increased expression levels of BmDJ-1 occur in the pupal developmental stage, which coincides with apoptosis and the apparent melting of the body. BmDJ-1 might be involved in the elimination of NO in metamorphosis.

Although DJ-1 protein acts as a controller caspase activation to alter self expression level in the apoptotic pathway [26], we cannot determine a direct relationship between BmDJ-1 and NO generation in metamorphosis based on these experiments.

In future studies, we will investigate whether BmDJ-1 directly regulates NO in metamorphosis.

Materials and Methods

Ethics statement

The study protocol for the experimental use of the animals was approved by the Ethics Committee of Meiji Pharmaceutical University (Approval ID 2004).

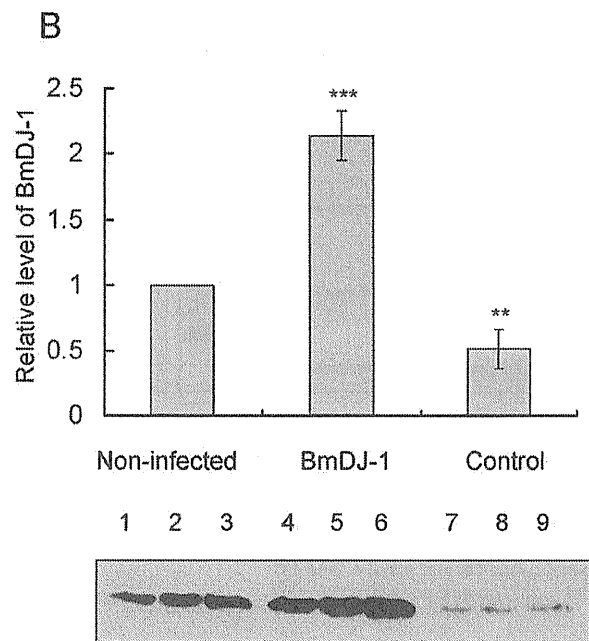
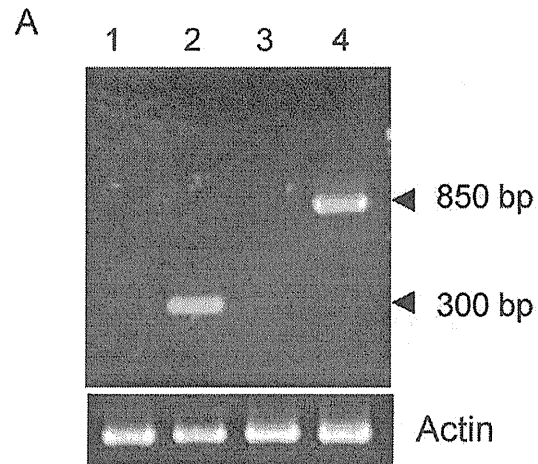


Figure 7. Expression of BmDJ-1 in silkworms infected by recombinant BmNPV. A. The fatbodies of several insects were dissected after 1 day (24 h) and 4 days (day 3 fifth instar larvae) and subjected to RT-PCR with BmNPV specific primers. Lanes 1, 2: blank virus; lanes 3, 4: recombinant virus; lanes 1, 3: 1 day after infection; lanes 2, 4: 4 days after infection. B. Aliquots (5 µg) of protein samples from fatbodies of several insects separated by SDS-PAGE, transferred to nitrocellulose, and probed with anti-BmDJ-1 antibody: non-infected control (day 3 fifth instar larvae) from experiments 1 (lane 1), 2 (lane 2) and 3 (lane 3); infected by recombinant virus from experiments 1 (lane 4), 2 (lane 5), 3 (lane 6); and blank virus after 4 days infection from experiments 1 (lane 7), 2 (lane 8), and 3 (lane 9). Protein level was measured by Image J ver 1.37 c and plotted to a graph. *P<0.05, **P<0.01 compared with control values. doi:10.1371/journal.pone.0017683.g007

Insects

The hybrid strain Kinshu x Showa was supplied from Ueda-Sha Co. Ltd., Nagano, Japan. Individuals were reared on the artificial diet Silkmate 2S (NOSAN, Tsukuba, Japan) and kept at 25°C on a 12 h light/12 h dark daily cycle.

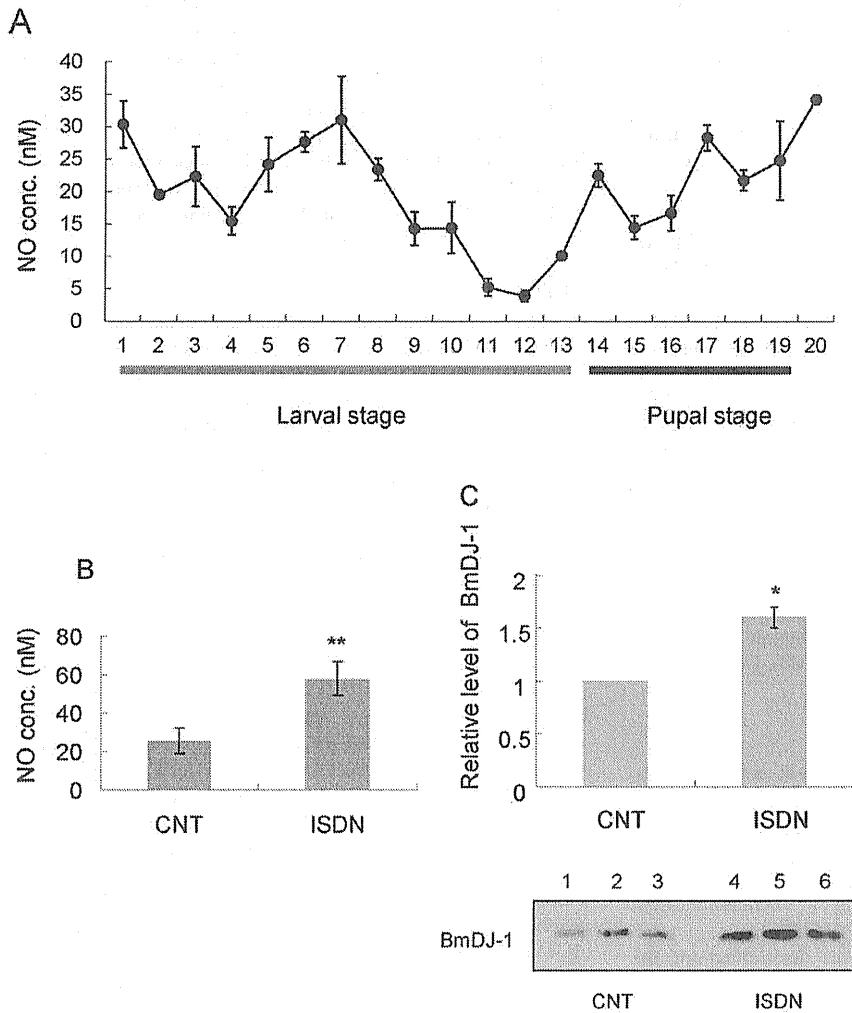


Figure 8. Change of NO concentration in hemolymph and expression of BmDJ-1 treated with ISDN. A. The hemolymph of several insects was collected from day 0 fifth instar larvae to adults and measured for NO concentration. 1–13: fifth instar larval stage (day 0 to 12); 14–19: pupal stage (day 0, 1, 3, 4, 7, 8); 20: adult. B. NO concentration in the medium. C. Aliquots (5 μ g) of protein samples from BmN4 cells, experiment 1 of control (lane 1), experiment 2 of control (lane 2), experiment 3 of control (lane 3), experiment 1 of ISDN treatment (lane 4), experiment 2 of ISDN treatment (lane 5), and experiment 3 of ISDN treatment (lane 6) were separated by SDS-PAGE, transferred to nitrocellulose, and probed with anti-BmDJ-1 antibody. Protein level was measured by Image J ver 1.37 c and plotted to a graph. * $P < 0.05$, ** $P < 0.01$ compared with control values. doi:10.1371/journal.pone.0017683.g008

Cell culture

An established silkworm cell line, BmN4 (NOSAN), was maintained at 25°C in TC-100 medium (NOSAN) supplemented with 10% fetal bovine serum and Antibiotic-Antimycotic (Invitrogen, Carlsbad, CA, USA).

Molecular cloning of BmDJ-1

We first searched the *B. mori* expressed sequence tag (EST) database on KAIKOBLAST (kaikoblast.dna.affrc.go.jp) using the *Drosophila melanogaster* DJ-1 alpha (NM_137072) or beta (NM_143568) sequence as a query, and identified the EST clone NRPG1136, which did not overlap the 5' end of the coding region of the *B. mori* DJ-1 gene (BmDJ-1). The entire coding sequence was determined using total RNA extracted from the brains of day 3 fifth instar larvae by an RNeasy mini kit (Qiagen, Valencia, CA, USA). DNase-treated total RNA was processed for cDNA

synthesis using oligo(dT)12-18 primers and SuperScript II reverse transcriptase (Invitrogen), and cDNA was amplified by PCR using Pfu Turbo DNA polymerase (Stratagene, La Jolla, CA, USA) and the primers 5'-TCAAGAACAATGAGCAAGTCTGCG-3' and 5'-TAATATTAGTACTGCGAGATTAAC-3'. The amplified products were cloned into a cloning vector p3T (MoBiTec, Göttingen, Germany). The purified vectors were processed for sequencing by the dideoxynucleotide chain termination method on an ABI PRIZM 3100 Genetic Analyzer (Applied Biosystems, Tokyo, Japan). The cDNA clone, NRPG1136, was provided by the National Bioresource Project (MEXT, Japan).

5'-Rapid Amplification of cDNA ends

The 5'-terminal cDNA ends were amplified using the SMART RACE cDNA Amplification kit (Clontech, Mountain View, CA, USA) according to the supplier's instructions with primers 5'-

GCCAGCTAGAGTAACTGTTACCCC-3' and 5'-AGTCAC-TTGCCCTTGAGCACAGCAC-3'. The amplified products were cloned into a p3T vector for sequencing.

Deduced amino acid sequences, were aligned and phylogenetic trees and homology analyses were done using BLAST (blast.genome.jp), CLC Free Workbench ver 3.2.3 (CLC Bio, Aarhus, Denmark), and Genetyx ver 9.0 (Genetyx Co., Tokyo, Japan).

Recombinant protein

The ORFs of BmDJ-1 were amplified by PCR using PfuTurbo DNA polymerase and primers 5'-AGCAAGTCTGCGTTAGT-GAT-3' and 5'-TTAGTACTGCGAGATTAACA-3'. Products were cloned into a prokaryotic expression vector pTrcHis-TOPO with a TOPO TA cloning kit (Invitrogen) and expressed in *E. coli* as fusion proteins with N-terminal Xpress tags. The nucleotide sequence was confirmed by sequencing. Recombinant BmDJ-1 expressed in *E. coli* was purified with HIS-Select spin columns (Sigma, St. Louis, MO, USA) according to methods described previously [27]. A recombinant β -galactosidase (LacZ) fragment tagged with Xpress included in the TOPO TA cloning kit was used as a negative control.

Immunology

The antibody for immunoblotting was raised in Japanese white rabbits by subcutaneous injection of the recombinant BmDJ-1 and Ribi adjuvant system (Corixa Co., Hamilton, MT, USA) mixture. The serum was stored at -80°C .

Immunoblotting

To identify the presence of BmDJ-1 in different tissues and cells, protein samples (5 μg) were separated on SDS-PAGE, transferred to nitrocellulose membranes using the method of Towbin *et al.* [28], and immunoblotted using rabbit anti-BmDJ-1 antibody and goat anti-rabbit IgG-conjugated horseradish peroxidase (HRP). The membranes were developed using a chemiluminescent substrate (Pierce, Rockford, IL, USA).

The tissue distribution of BmDJ-1 was determined for the midgut, fatbody, Malpighian tubule, testis, and ovary from day 0 fifth instar larvae, pupae, and adults. Each tissue sample was run on the same gel, which was also loaded with 20 ng of recombinant Xpress-tagged BmDJ-1. The distribution of BmDJ-1 from first to fifth instar larvae, pupae and adult on the whole body and brain of larvae, pupae and adults were also determined. All tissues were homogenized in RIPA lysis buffer composed of 50 mM Tris-HCl, pH 7.5, 150 mM NaCl, 1% Nonidet P40, 0.5% sodium deoxycholate, 0.1% SDS, and a cocktail of protease inhibitors (Sigma), followed by centrifugation at $10,000\times g$ for 15 min.

The protein concentration was determined by a Bradford assay kit (Pierce). Samples of supernatant (5 μg of protein) were separated by SDS-PAGE, transferred to nitrocellulose membranes, and immunoblotted with anti-BmDJ-1 antibody following the procedure described above.

Specificity of antibody against BmDJ-1

We examined the specificity of antibody against BmDJ-1 using following samples: 0.25 or 0.5 μg recombinant BmDJ-1 protein with xpress tag, 1 μg recombinant CBP protein with GST tag [21], 10 μg HEK293 cell lysate, BmN4 cell lysate and 10 μg larva brain lysate.

Northern blot analysis

Total RNA derived from the ovaries of day 4 fifth instar larvae were used. Total RNA (12 μg) was separated on a 1.5% agarose-

6% formaldehyde gel and transferred to a nylon membrane. DIG-labeled probes were synthesized using the PCR DIG probe synthesis kit (Roche Diagnostics, Mannheim, Germany) according to the supplier's instructions with the primers 5'-CATTT-GTGCTGCTTCCATAGCGTT-3' and 5'-CATTCCCTTTT-CGACTTGATCGGC-3'. After pre-hybridization, the membranes were hybridized with the DIG-labeled probes at 54°C overnight. The specific reaction was visualized on Kodak X-OMAT AR X-ray films by the DIG chemiluminescence detection kit (Roche Diagnostics).

RT-PCR

Total RNA derived from the brain, midgut, fatbody, Malpighian tubule, testis, ovary, and hemocyte of day 4 fifth instar larvae was DNase-treated and processed for cDNA synthesis using oligo(dT)12–18 primers and SuperScript II reverse transcriptase (Invitrogen). cDNA was amplified by PCR using Taq DNA polymerase (Qiagen) and the primers 5'-CATTTGTGCTG-GTTCATAGCGTT-3' and 5'-CATTCCCTTTTTCGACTT-GATCGGC-3'. Amplification was carried out for 30 cycles of denaturing for 40 s at 94°C , annealing for 40 s at 50°C and extension for 90 s at 72°C . Amplified PCR products were separated by agarose gel, stained with ethidium bromide, and visualized under UV light.

Transfer plasmid and generation of recombinant virus

The ORF sequence of BmDJ-1 was amplified by PCR from brain cDNA as described above, with the primers 5'-GGG-GTACCCCATGAGCAAGTCTGCGTTAGTGAT-3' and 5'-GGAATTCGAATATTAGTACTGCGAGATTAAC-3'. The amplified region was digested with EcoRI and KpnI and cloned into the baculovirus transfer pBK283 vector. Blank pBK283 vector was used as a control. For generating recombinant BmNPV, we used a Bom-EX kit (NOSAN) according to the supplier's instructions. The recombinant BmNPV nucleotide sequence was confirmed by sequencing using the primers 5'-ACTGTGACAAGCTCTGTCC-3' and 5'-ACAACGCACA-GAATCTAACGC-3'. Purified recombinant virus was titrated by plaque assay, and high titer stocks (2×10^7 pfu/ml) were used for infecting larvae.

Determination of LD₅₀ of day 4 fifth instar larvae by ROT stimulation

To determine the LD₅₀ of day 3 fifth instar larvae by ROT (Sigma) stimulation, we injected ROT intrahemocoelically to larvae weighing 3.5 to 4.0 g using a disposable syringe (Terumo, Tokyo, Japan) with a 30G needle. ROT was dissolved in DMSO (prepared immediately before use and stored in the dark) at 0, 1.25, 2.5, 5.0, 10, 20, 40, and 80 $\mu\text{g}/\text{g}$ and injected into larvae in a volume of 10 $\mu\text{l}/\text{g}$ body weight. The number of dead silkworms after 24 h was counted and the mortality rate (%) = $(X/Y)\times 100$ was calculated, where X = dead larvae in the group and Y = total larvae in the group. The mortality rates were analyzed with Probit analyses [29] using the Probit Analysis option in the SAS 8.2 software package (SAS Institute Japan Ltd., Tokyo, Japan) to calculate the LD₅₀.

Overexpression of BmDJ-1 to larvae and exposure to ROT oxidative stimuli

A 50 μl aliquot of BmNPV-BmDJ-1 or BmNPV-blank-vector (1×10^3 pfu/larva) was injected intrahemocoelically into day 0 fifth instar larvae using a disposable syringe (Terumo) with a 30G needle. Blank-vector recombinant virus was injected as a control.

After rearing for 4 days on an artificial diet, larvae were examined for overexpression of BmDJ-1 to assess protection from oxidative stress due to ROT.

Virus-derived BmDJ-1 expression level was measured in the dissected fatbodies of several insects after 1 day (24 h) and 4 days (day 3 fifth instar) by RT-PCR with the primers 5'-ACTGTC-GACAAGCTCTGTCC-3' and 5'-ACAACGCACAGAATCTAACGC-3'.

Virus-derived BmDJ-1 expression level was measured in the dissected fatbodies of several insects after 4 days (day 3 fifth instar) by immunoblotting.

We surmised the ROT dose that would be most effective in the experimental model with exogenous BmDJ-1 based on a report of the administration of exogenous DJ-1 [30].

ROT, prepared at 20 $\mu\text{g/g}$ (LD_{70}), was injected to three groups of 10 to 20 larvae in a volume of 10 $\mu\text{l/g}$ body weight. The number of dead silkworms after 24 h was counted and the mortality rate (%) was calculated.

Data were analyzed with the multiple comparison test followed by the Cochran-Armitage test for dose-response relationship and Steel's (non-parametric) multiple comparison test. $P < 0.05$ was considered significant. All statistical analyses were carried out using SAS system 8.2 software. Three trials were performed in each experiment.

BmN4 cells treated with ROT, two-dimensional (2D) gel electrophoresis, and detection of BmDJ-1

BmN4 cells (2×10^6) were grown on 6-well Falcon plates (BD Biosciences, Franklin Lakes, NJ, USA) and washed twice with PBS followed by 3 h of treatment with TC-100 medium containing ROT (50 μM) dissolved in 0.1% DMSO or 0.1% DMSO as a control in the dark. To prepare total protein extracts for two-dimensional (2D) gel electrophoretic analysis, the cells were sonicated in rehydration buffer comprising 8 M urea, 2% CHAPS, 0.5% carrier ampholytes at pH 3–10, 20 mM dithiothreitol, 0.002% bromophenol blue, and a cocktail of protease inhibitors. Urea-soluble proteins were separated by isoelectric focusing (IEF) using the ZOOM IPGRunner system loaded with an immobilized pH 3–10 gradient strip (Invitrogen), as described previously [16]. After the first dimension of IEF, the protein was separated in the second dimension on a 4–12% NuPAGE polyacrylamide gel (Invitrogen). For detection of BmDJ-1, the gel was transferred to a polyvinylidene difluoride (PVDF) membrane for immunoblotting.

All incubation steps were carried out at 25°C in the dark. Three trials were performed for each experiment.

Collection of samples and measurement of NO levels

Hemolymph (250 μl) was collected from day 0 fifth instar larvae, pupae and adults, or from medium to measure the concentration of NO. To remove proteins, samples were mixed with methanol (2:1 by volume), followed by centrifugation at $10,000 \times g$ for 20 min, and NO levels in the supernatants were measured using an NOx analyzer (ENO-20; Eicom, Kyoto, Japan), according to the manual.

References

- Bandyopadhyay S, Cookson MR (2004) Evolutionary and functional relationships within the DJ1 superfamily. *BMC Evol Biol* 4: 1–9.
- Costa CA (2007) DJ-1: a newcomer in Parkinson's disease pathology. *Curr Mol Med* 7: 650–657.
- Kinumi T, Kimata J, Taira T, Ariga H, Nikia E (2004) Cysteine-106 of DJ-1 is the most sensitive cysteine residue to hydrogen peroxide-mediated oxidation in vivo in human umbilical vein endothelial cells. *Biochem Biophys Res Commun* 317: 722–728.
- Bové J, Prou D, Perier C, Przedborski S (2005) Toxin-induced models of Parkinson's disease. *NeuroRx* 2: 484–494.
- Terzioglu M, Galter D (2008) Parkinson's disease: genetic versus toxin-induced rodent models. *FEBS J* 275: 1384–1391.
- Panov A, Dikalov S, Shalbuyeva N, Taylor G, Sherer T, et al. (2005) Rotenone model of Parkinson disease: multiple brain mitochondria dysfunctions after short term systemic rotenone intoxication. *J Biol Chem* 280: 42026–42035.

BmN4 cell treatment with ISDN and detection of BmDJ-1

BmN4 cells (2×10^6) were grown on 6-well Falcon plates (BD Biosciences) and washed twice with PBS followed by 16 h of treatment with TC-100 medium containing 100 μM of isosorbide dinitrate (ISDN; prepared immediately prior to use and kept in the dark) dissolved in 0.1% ethanol or with 0.1% ethanol alone as a control. Total protein extracts were prepared for immunoblotting and culture medium was prepared for NO analysis. Statistical analysis was performed using Student's *t*-test. $P < 0.05$ was considered significant. All statistical analyses were carried out using SAS system 8.2 software. Three trials were performed for each experiment.

Supporting Information

Figure S1 SDS-PAGE and CBB staining of figure 4. A. Whole body homogenates from day 0 larvae of the first (lane 1), second (lane 2), third (lane 3), fourth (lane 4), and fifth (lane 5) instars, the pupae (lane 6), and the adult (lane 7). B, Brain of the fifth instar larvae (lane 8), pupae (lane 9), and adults (lane 10). C. a, midgut; b, fatbody; c, Malpighian tubule; d, testis; and e, ovary were isolated from day 0 to 12 fifth instar larvae (lanes 1 to 13), from day 0, 1, 3, 4, 7 and 8 pupae (lanes 14 to 19), and from day 0 adults (lane 20). No samples were loaded in panel a, lanes 17, 18, 19, 20; panel c, lane 16; and panel e, lane 13. (TIFF)

Figure S2 SDS-PAGE and CBB staining of figure 7B. Non-infected control (day 3 fifth instar larvae) from experiments 1 (lane 1), 2 (lane 2) and 3 (lane 3); infected by recombinant virus from experiments 1 (lane 4), 2 (lane 5), 3 (lane 6); and blank virus after 4 days infection from experiments 1 (lane 7), 2 (lane 8), 3 (lane 9). (TIFF)

Figure S3 SDS-PAGE and CBB staining of figure 8C. Experiment 1 of control (lane 1), experiment 2 of control (lane 2), experiment 3 of control (lane 3), experiment 1 of ISDN treatment (lane 4), experiment 2 of ISDN treatment (lane 5), and experiment 3 of ISDN treatment (lane 6). (TIFF)

Acknowledgments

We are indebted to Dr. Taro Tamaki for critical reading of the manuscript, Dr. Yuki Ogasawara for advice on the oxidative stress experiment, Dr. Kikuo Iwabuchi for advice on cell culture, and Ms. Mai Ikeda, Ms. Hiroko Nakano and Ms. Yukiko Senoh for technical assistance.

Author Contributions

Conceived and designed the experiments: HT JS. Performed the experiments: HT HO SK KY. Analyzed the data: TS KM. Contributed reagents/materials/analysis tools: YB RS. Wrote the paper: HT. Measurement of NO levels: RIN.

7. Menzies FM, Yeniseti SC, Min KT (2005) Roles of *Drosophila* DJ-1 in survival of dopaminergic neurons and oxidative stress. *Curr Biol* 15: 1578–1582.
8. Olzmann JA, Brown K, Wilkinson KD, Rees HD, Huai Q, et al. (2004) Familial Parkinson's disease-associated L166P mutation disrupts DJ-1 protein folding and function. *J Biol Chem* 279: 8506–8515.
9. Tao X, Tong L (2003) Crystal structure of human DJ-1, a protein associated with early onset Parkinson's disease. *J Biol Chem* 278: 31372–31379.
10. Anderson PC, Daggett V (2008) Molecular basis for the structural instability of human DJ-1 induced by the L166P mutation associated with Parkinson's disease. *Biochemistry* 47: 9380–9393.
11. Blackinton J, Lakshminarasimhan M, Thomas KJ, Ahmad R, Greggio E, et al. (2009) Formation of a stabilized cysteine sulfinic acid is critical for the mitochondrial function of the parkinsonism protein DJ-1. *J Biol Chem* 284: 6476–6485.
12. Meulener MC, Xu K, Thomson L, Ischiropoulos H, Bonini NM (2004) Mutational analysis of DJ-1 in *Drosophila* implicates functional inactivation by oxidative damage and aging. *Proc Natl Acad Sci USA* 103: 12517–12522.
13. Mita K, Kasahara M, Sasaki S, Nagayasu Y, Yamada T, et al. (2004) The genome sequence of silkworm, *Bombyx mori*. *DNA Res* 11: 27–35.
14. Ohnishi A, Hull JJ, Matsumoto S (2006) Targeted disruption of genes in the *Bombyx mori* sex pheromone biosynthetic pathway. *Proc Natl Acad Sci USA* 103: 4398–4403.
15. Tomita M, Munetsuna H, Sato T, Adachi T, Hino R, et al. (2003) Transgenic silkworms produce recombinant human type III procollagen in cocoons. *Nat Biotechnol* 21: 52–56.
16. Xia Q, Zhou Z, Lu C, Cheng D, Dai F, et al. (2004) A draft sequence for the genome of the domesticated silkworm (*Bombyx mori*). *Science* 306: 1937–1940.
17. Xia Q, Cheng D, Duan J, Wang G, Cheng T, et al. (2007) Microarray-based gene expression profiles in multiple tissues of the domesticated silkworm, *Bombyx mori*. *Genome Biol* 8: R162.
18. Kozak M (1984) Compilation and analysis of sequences upstream from the translational start site in eukaryotic mRNAs. *Nucleic Acids Res* 12: 857–872.
19. Pedersen AG, Nielsen H (1997) Neural network prediction of translation initiation sites in eukaryotes: perspectives for EST and genome analysis. *Proc Int Conf Intell Syst Mol Biol* 5: 226–233.
20. Yamamoto K, Narukawa J, Kadono-Okuda K, Nohata J, Sasanuma M, et al. (2006) Construction of a single nucleotide polymorphism linkage map for the silkworm, *Bombyx mori*, based on bacterial artificial chromosome end sequences. *Genetics* 173: 151–161.
21. Tabunoki H, Sugiyama H, Tanaka Y, Fujii H, Banno Y, et al. (2002) Isolation, characterization, and cDNA sequence of a carotenoid binding protein from the silk gland of *Bombyx mori* larvae. *J Biol Chem* 277: 32133–32140.
22. Meulener M, Whitworth A J, Armstrong-Gold CE, Rizzo P, Heutink P, et al. (2007) *Drosophila* DJ-1 mutants are selectively sensitive to environmental toxins associated with Parkinson's disease. *Curr Biol* 15: 1572–1577.
23. Maeda S, Kawai T, Obinata M, Fujiwara H, Horiuchi T, et al. (1985) Production of human alpha-interferon in silkworm using a baculovirus vector. *Nature* 315: 592–594.
24. Choi SK, Choi HK, Kadono-Okuda K, Taniaki K, Kato Y, et al. (1995) Occurrence of novel types of nitric oxide synthase in the silkworm, *Bombyx mori*. *Biochem Biophys Res Commun* 207: 452–459.
25. Inoue M, Sato EF, Nishikawa M, Hiramoto K, Kashiwagi A, et al. (2004) Free radical theory of apoptosis and metamorphosis. *Redox Rep* 9: 237–247. Review.
26. Fan J, Ren H, Jia N, Fei E, Zhou T, et al. (2008) DJ-1 decreases Bax expression through repressing p53 transcriptional activity. *J Biol Chem* 283: 4022–4030.
27. Tabunoki H, Shimada T, Banno Y, Sato R, Kajiwara H, et al. (2008) Identification of *Bombyx mori* 14-3-3 orthologs and the interactor Hsp60. *Neurosci Res* 61: 271–280.
28. Towbin H, Staehelin J, Gordon J (1979) Electrophoretic transfer of proteins from polyacrylamide gels to nitrocellulose sheets: procedure and some applications. *Proc Natl Acad Sci USA* 76: 4350–4354.
29. Finny DJ (1947) *Probit Analysis: A Statistical Treatment of the Sigmoid Response Curve*. Cambridge, NY: Cambridge University Press. 20 p.
30. Inden M, Taira T, Kitamura Y, Yanagida T, Tsuchiya D, et al. (2006) PARK7 DJ-1 protects against degeneration of nigral dopaminergic neurons in Parkinson's disease rat model. *Neurobiol Dis* 24: 144–158.

Original Article

Immunohistochemical characterization of microglia in Nasu-Hakola disease brains

Jun-ichi Satoh,¹ Hiroko Tabunoki,¹ Tsuyoshi Ishida,² Saburo Yagishita,³ Kenji Jinnai,⁴
Naonobu Futamura,⁴ Michio Kobayashi,⁵ Itaru Toyoshima,⁶ Toshiaki Yoshioka,⁷
Katsuhiko Enomoto,⁷ Nobutaka Arai⁸ and Kunimasa Arima⁹

¹Department of Bioinformatics and Molecular Neuropathology, Meiji Pharmaceutical University, ⁸Department of Clinical Neuropathology, Tokyo Metropolitan Institute for Neuroscience, ⁹Department of Psychiatry, National Center Hospital, NCNP, Tokyo, ²Department of Pathology and Laboratory Medicine, Kohnodai Hospital, National Center for Global Health and Medicine, Chiba, ³Department of Pathology, Kanagawa Rehabilitation Center, Kanagawa, ⁴Department of Neurology, Hyogo-Cyuo National Hospital, Hyogo, ⁵Department of Neurology, Akita National Hospital, ⁶Department of Neurology and Medical Education Center, Akita University School of Medicine and ⁷Department of Molecular Pathology and Tumor Pathology, Akita University School of Medicine, Akita, Japan

Nasu-Hakola disease (NHD) is a rare autosomal recessive disorder, characterized by progressive presenile dementia and formation of multifocal bone cysts, caused by genetic mutations of DNAX-activation protein 12 (DAP12) or triggering receptor expressed on myeloid cells 2 (TREM2). TREM2 and DAP12 constitute a receptor/adaptor signaling complex expressed on osteoclasts, dendritic cells (DC), macrophages and microglia. Previous studies using knock-out mice and mouse brain cell cultures suggest that a loss-of-function of DAP12/TREM2 in microglia plays a central role in the neuropathological manifestation of NHD. However, there exist no immunohistochemical studies that focus attention on microglia in NHD brains. To elucidate a role of microglia in the pathogenesis of NHD, we searched NHD-specific biomarkers and characterized their expression on microglia in NHD brains. Here, we identified allograft inflammatory factor 1 (AIF1, Iba1) and sialic acid binding Ig-like lectin 1 (SIGLEC1) as putative NHD-specific biomarkers by bioinformatics analysis of microarray data of NHD DC. We studied three NHD and eight control brains by immunohistochemistry with a panel of 16 antibodies, including those against Iba1 and SIGLEC1. We verified the absence of DAP12 expression in NHD brains and the expression of DAP12 immunoreactivity on

ramified microglia in control brains. Unexpectedly, TREM2 was not expressed on microglia but expressed on a small subset of intravascular monocytes/macrophages in control and NHD brains. In the cortex of NHD brains, we identified accumulation of numerous Iba1-positive microglia to an extent similar to control brains, while SIGLEC1 was undetectable on microglia in all the brains examined. These observations indicate that human microglia in brain tissues do not express TREM2 and DAP12-deficient microglia are preserved in NHD brains, suggesting that the loss of DAP2/TREM2 function in microglia might not be primarily responsible for the neuropathological phenotype of NHD.

Key words: bioinformatics, DAP12, microglia, Nasu-Hakola disease, TREM2.

INTRODUCTION

Nasu-Hakola disease (NHD; OMIM 221770), also designated polycystic lipomembranous osteodysplasia with sclerosing leukoencephalopathy (PLOS), is a rare autosomal recessive disorder, characterized by progressive presenile dementia and formation of multifocal bone cysts filled with convoluted adipocyte membranes.^{1,2} The clinical course of NHD is classified into four stages: (i) the latent stage with normal early development; (ii) the osseous stage beginning at the third decade of life, presenting with pain and swelling of ankles and feet followed by pathological bone fractures; (iii) the early neuropsychiatric stage occurring at the fourth decade of life, presenting with a frontal lobe syndrome such

Correspondence: Jun-ichi Satoh, MD, Department of Bioinformatics and Molecular Neuropathology, Meiji Pharmaceutical University, 2-522-1 Noshio, Kiyose, Tokyo 204-8588, Japan. Email: satoj@my-pharm.ac.jp

Received 23 July 2010; revised and accepted 27 September 2010; published online 1 December 2010.

as euphoria and loss of social inhibitions; and (iv) the late neuropsychiatric stage, presenting with profound dementia, loss of mobility and death usually by age 50 years.³ The neuropathological hallmark of NHD includes profound loss of myelin and axons, and accumulation of axonal spheroids and sudanophilic granules, accompanied by intense astrogliosis predominantly in the frontal and temporal lobes and the basal ganglia.^{4,5}

Nasu-Hakola disease is caused by a structural defect in one of the two genes, DNAX-activation protein 12 (DAP12), alternatively named TYRO protein tyrosine kinase-binding protein (TYROBP) on chromosome 19q13.1, or triggering receptor expressed on myeloid cells 2 (TREM2) on chromosome 6p21.1. Seventeen different NHD-causing loss-of-function mutations currently identified in either DAP12 or TREM2 cause an identical disease phenotype.^{6,7} DAP12 is expressed as a disulfide-bonded homodimer on natural killer (NK) cells, monocytes/macrophages, dendritic cells (DC), osteoclasts, and brain microglia. DAP12 constitutes a transmembrane adaptor that noncovalently associates with several cell-surface receptors, including natural cytotoxicity triggering receptor 2 (NCR2), TREM2, TREM1, signal-regulatory protein beta 1 (SIRPB1), and myeloid DAP12-associating lectin 1 (MDL1), and transmits either activating or inhibitory signals depending on the avidity of their ligands.⁸ DAP12-deficient mice develop osteopetrosis, hypomyelinoses accentuated in the thalamus, and synaptic degeneration, suggesting that DAP12 signaling is essential for development of osteoclasts and oligodendrocytes and synaptogenesis.⁹ DAP12-deficient macrophages produced higher concentrations of inflammatory cytokines in response to toll-like receptor (TLR) stimulation.¹⁰ The synaptic function is altered in DAP12 loss-of-function mice due to reduced expression of AMPA receptor GluR2 subunit and TrkB.¹¹ Furthermore, the number of microglia is greatly reduced in the brain of DAP12-deficient/loss-of-function mice.^{12,13}

TREM2 is expressed on osteoclasts, DC, macrophages and microglia, and recognizes polyanionic macromolecules, bacteria and heat shock protein HSP60.¹⁴⁻¹⁷ Apoptotic neuronal cell membranes express endogenous TREM2 ligands.¹⁸ Crosslinking of TREM2 on cultured mouse microglia triggers phagocytosis of apoptotic neurons without secretion of proinflammatory cytokines, while knockdown of TREM2 inhibits phagocytosis of apoptotic neurons and stimulates production of proinflammatory cytokines such as TNF and IL-1 β .¹⁹ These observations suggest the hypothesis that the pathogenesis of NHD is mainly attributable to the inability of DAP12/TREM2-deficient microglia to remove apoptotic neurons, followed by enhanced production of proinflammatory cytokines in the brain. However, at present, the precise role of microglia

in persistent demyelination, gliosis and axonal degeneration in NHD brains, caused by loss of function of DAP12/TREM2, remains largely unknown. There exist no immunohistochemical studies that focus attention on microglia in NHD brains.

To investigate an active role of microglia in the neuropathological manifestation of NHD, first we attempted to identify NHD-specific biomarker genes by *in silico* bioinformatics analysis of microarray data. Then, we studied three NHD brains, compared with eight control brains side by side, by immunohistochemistry using a panel of antibodies against cell type-specific markers and putative disease-specific biomarkers.

MATERIALS AND METHODS

Hierarchical clustering analysis of microarray data

The microarray dataset GSE3624 was downloaded from of the Gene Expression Omnibus (GEO) repository (<http://www.ncbi.nlm.nih.gov/geo>). In this dataset, RNA was prepared from peripheral blood monocyte-derived dendritic cells (DC) induced by IL-4 and GM-CSF isolated from three NHD patients with DAP12 mutation of EX1-4 DEL, two NHD patients with TREM2 mutation of either Q33X or V126G, and three normal control (NC) subjects.²⁰ The gene expression profile was analyzed by the Affymetrix Human Genome HG-U133A chip containing 22 283 transcripts, and the data were normalized following the Microarray Analysis Suite 5.0 (MAS5: Affymetrix, Santa Clara, CA, USA) algorithm. To identify NHD DC-specific biomarker genes, we selected 226 differentially expressed genes (DEGs) by comparing the transcriptome data among DAP12-mutated patients, TREM2-mutated patients, and NC subjects with one-way analysis of variance (ANOVA) ($P < 0.001$). Among them, we extracted 73 DEGs showing the changes in expression levels greater than 2-fold or smaller than 0.5-fold in DAP12-mutated patients versus NC subjects, after omitting the genes called as absent (A) or marginal (M). Then, these data were imported into the Cluster 3.0 software (bonsai.ims.u-tokyo.ac.jp/~mdehoon/software/cluster), followed by visualizing them on Java TreeView1.1.3 (sourceforge.net/projects/jtreeview).

Molecular network analysis

Ingenuity Pathways Analysis (IPA) 8.5 is a knowledgebase that contains approximately 2 270 000 biological and chemical interactions and functional annotations with scientific evidence. They are collected from more than 500 selected articles, textbooks and other data sources, manu-

Table 1 Primary antibodies utilized for immunohistochemistry

Antibody	Supplier	Code (ID)	Origin	Antigen	Concentration
DAP12	Santa Cruz Biotechnology	sc-20783 (FL-113)	Rabbit	Full-length human DAP12 protein	1:500
TREM2	Sigma	HPA010917	Rabbit	A peptide composed of AAWHGQKPGTHPPSELDCG HDPGYQLQTLPLGRDT	1:100
TREM1	Sigma	HPA005563	Rabbit	A peptide composed of PGSNENSTQNVYKIPPTTKAL CPLYTSPRTVTQAPPKSTADVS TPDSEINLTNVTDI	1:250
IBA1	Wako	019-19741	Rabbit	A synthetic peptide corresponding to the C-terminus of Iba1	1:2000
HLA-DR	Dako	M0746 (TAL.1B5)	Mouse	The α -chain subunit of HLA class II DR antigens	1:100
CD68	Dako	N1577 (KP1)	Mouse	Lysosomal granules of human lung macrophages	Prediluted
CD163	Novocastra	NCL-CD163 (10D6)	Mouse	Recombinant human CD163 protein corresponding to domains of 1 to 4 of the N-terminal region	1:50 of the hybridoma culture supernatant
MSR1	Transgenic	KT022 (SRA-E5)	Mouse	Recombinant human MSR1 (CD204) protein	1:100
SIGLEC1	Santa Cruz Biotechnology	sc-53442 (HSn7D2)	Mouse	Fc fusion protein containing N-terminal 4 domains of human Siglec1	1:20
SIRPB1	Proteintech Group	11811-1-AP	Rabbit	Recombinant human SIRBP1 protein	1:1000
GFAP	Dako	N1506	Rabbit	GFAP purified from bovine spinal cord	Prediluted
MBP	Dako	N1564	Rabbit	MBP purified from human brain	Prediluted
NF	Nichirei	412551 (2F11)	Mouse	NF purified from human brain	Prediluted
SYNAP	Novocastra	NCL-SYNAP-299 (27G12)	Mouse	A synthetic peptide corresponding to the region close to the C-terminus of synaptophysin	1:500 of the hybridoma culture supernatant
CD3	Nichirei	413241 (PS1)	Mouse	Recombinant human CD3 epsilon chain protein	Prediluted
Cleaved Caspase-3	Cell Signaling Technology	#9661 (Asp175)	Rabbit	A peptide mapping amino-terminal residues adjacent to Asp175 of human caspase-3	1:100

GFAP, glial fibrillary acidic protein; MBP, myelin basic protein; MSR1, macrophage scavenger receptor 1; NF, neurofilament protein; SIGLEC1, sialic acid binding Ig-like lectin 1; SIRPB1, signal-regulatory protein beta 1; SYNAP, synaptophysin; HLA-DR, human leukocyte antigen MHC class II DR.

ally curated by expert biologists. By uploading the gene list, the network-generation algorithm identifies focused genes integrated in a global molecular network.²¹ IPA calculates the *P*-value, the statistical significance of association between the genes and the network by Fisher's exact test.

Human brain tissues

The brain tissues were obtained from Research Resource Network (RRN), Tokyo, Japan. Written informed consent at autopsy was obtained for all cases, following the regulations of the institutional ethics committees. The present study includes three patients with NHD, composed of a 42-year-old man (NHD1), a 48-year-old woman (NHD2), and a 44-year-old man (NHD3), four patients with myotonic dystrophy (MD) selected as neurological disease con-

trols, composed of a 68-year-old man (MD1), a 61-year-old man (MD2), a 60-year-old man (MD3) and a 53-year-old woman (MD4), and four subjects who died of non-neurological causes (NC), composed of a 63-year-old man who died of prostate cancer and acute myocardial infarction (NC1), a 67-year-old man who died of dissecting aortic aneurysm (NC2), a 57-year-old man who died of alcoholic liver cirrhosis (NC3) and a 61-year-old man who died of rheumatoid arthritis with interstitial pneumonia (NC4). The brain regions include the frontal cortex, the hippocampus and the basal ganglia in NHD cases, and the frontal cortex and the hippocampus in MD and NC cases. The homozygous mutation of a single base deletion of 141G (141delG) in exon 3 of DAP12 was identified in NHD1 and NHD2, while the genetic analysis was not performed in NHD3.

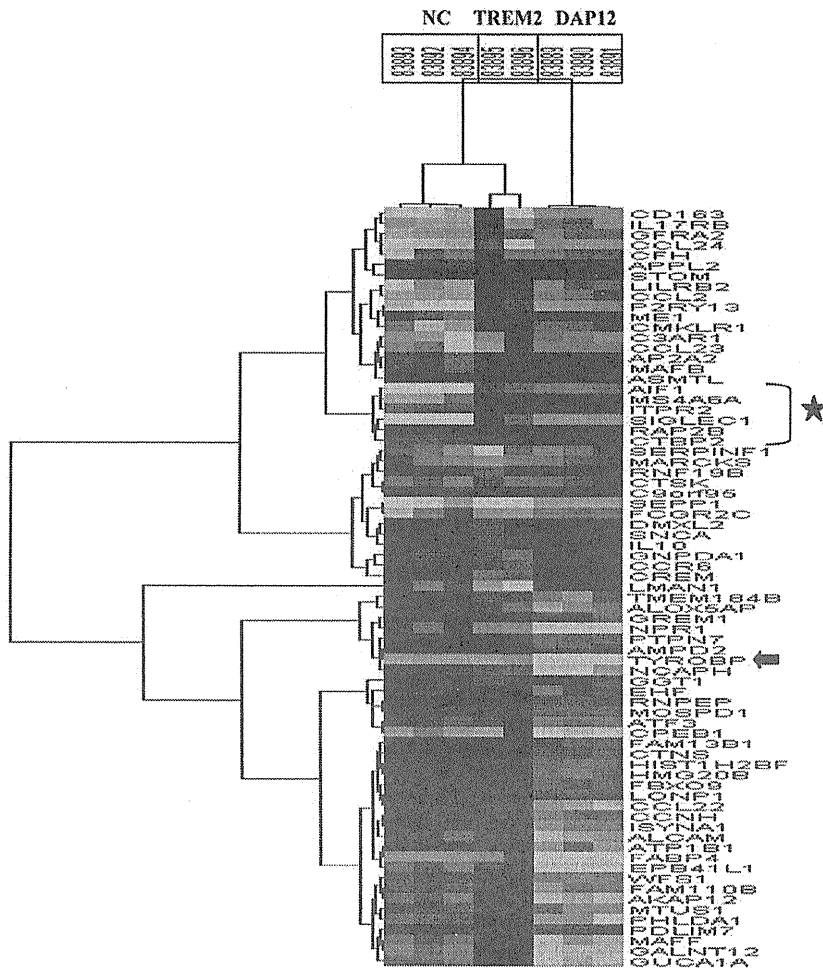


Fig. 1 Hierarchical clustering analysis of transcriptome data of dendritic cells isolated from Nasu-Hakola disease (NHD) patients. The dataset GSE3624 is composed of genome-wide transcriptome data of dendritic cells (DC) isolated from three DNAX-activation protein 12 (DAP12)-mutated patients, two triggering receptors expressed on myeloid cells 2 (TREM2)-mutated patients, and three normal control (NC) subjects. By bioinformatics analysis of this dataset, we identified 73 genes differentially expressed in DC of DAP12-mutated patients. They were processed for hierarchical clustering analysis. In the heat map, red and green colors represent upregulation or downregulation, respectively. TYROBP (DAP12) is indicated by an arrow. Six NHD-specific biomarker candidates (AIF1, MS4A6A, ITPR2, SIGLEC1, RAP2B and CTBP2) are bracketed by a star.

Immunohistochemistry

After deparaffination, tissue sections were heated in 10 mmol/L citrate sodium buffer by autoclave at 125°C for 30 s in a temperature-controlled pressure chamber (Dako, Tokyo, Japan). They were exposed to 3% hydrogen peroxide-containing methanol at room temperature (RT) for 15 min to block the endogenous peroxidase activity. The tissue sections were then incubated with PBS containing 10% normal goat serum at RT for 15 min to block non-specific staining. They were incubated in a moist chamber at 4°C overnight with primary antibodies listed in Table 1. Among the primary antibodies utilized, we validated the specificity of anti-TREM2 antibody and anti-DAP12 antibody by Western blot analysis of protein extract of HEK293 cells expressing corresponding recombinant proteins. After washing with PBS, the tissue sections were labeled at RT for 30 min with a horseradish peroxidase (HRP)-conjugated secondary antibody (Nichirei, Tokyo, Japan), followed by incubation with a coloring solution containing diaminobenzidine tetrahydrochloride

(DAB). For double immunolabeling, the incubation of primary antibodies was followed by incubation with alkaline phosphatase (AP)-conjugated secondary antibody (Nichirei), and colored with New Fuchsin substrate. All the sections were exposed to a counterstain with hematoxylin. For negative controls, the step of incubation with primary antibodies was omitted.

RESULTS

Bioinformatics approach identified molecular biomarkers and networks in DC of NHD

The dataset GSE3624 is composed of genome-wide transcriptome data of peripheral blood monocyte-derived DC expanded *in vitro* isolated from three DAP12-mutated patients, two TREM2-mutated patients and three NC subjects.²⁰ By reanalyzing the dataset with one-way ANOVA, we identified 226 differentially expressed genes (DEGs) among DAP12-mutated, TREM2-mutated and NC groups.

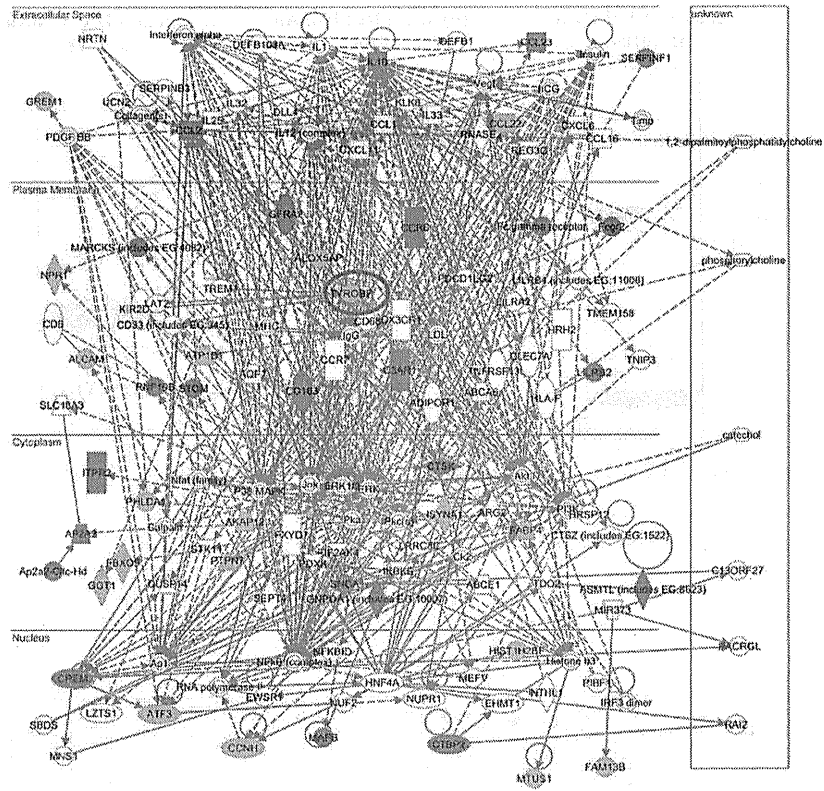


Fig. 2 Molecular network of 73 genes differentially expressed in dendritic cells of DNAX-activation protein 12 (DAP12)-mutated patients. The molecular network of 73 genes differentially expressed in dendritic cells (DC) of DAP12-mutated patients was analyzed by Ingenuity Pathways Analysis (IPA). It constitutes a highly complex network that has the most significant relationship with inflammatory response, cell signaling, and molecular transport. Red and green nodes represent upregulated or down-regulated genes, respectively. TYROBP (DAP12) is enclosed by a blue circle.

From these, we extracted 73 DEGs, either upregulated or downregulated in DAP12-mutated patients. Hierarchical clustering analysis of 73 DEGs produced a heat map showing that the expression of TYROBP (DAP12) was greatly reduced in DC of DAP12-mutated patients, while it was preserved in those of TREM2-mutated patients and NC subjects (Fig. 1, arrow). Importantly, a panel of genes composed of allograft inflammatory factor 1 (AIF1), alternatively named ionized calcium-binding adapter molecule 1 (Iba1), membrane-spanning 4-domains, subfamily A, member 6A (MS4A6A), inositol 1,4,5-triphosphate receptor, type 2 (ITPR2), sialic acid binding Ig-like lectin 1 (SIGLEC1), RAP2B, member of RAS oncogene family (RAP2B), and C-terminal binding protein 2 (CTBP2) were upregulated in DC of both DAP12-mutated and TREM2-mutated patients compared with NC subjects, suggesting that the six genes represent a candidate for NHD-specific biomarker molecules (Fig. 1, star). Because previous studies reported that microglia express Iba1 and SIGLEC1,^{22,23} we selected both for immunohistochemical analysis.

The molecular network analysis of 73 DEGs by IPA showed a highly complex network that has the most significant relationship with inflammatory response, cell signaling, and molecular transport ($P = 1.00E-67$), suggesting that aberrantly expressed genes in DAP12-mutated DC

involve dysregulation of a wide range of inflammatory signaling events (Fig. 2).

Preservation of microglia in the brains of NHD

We studied the tissue section of the frontal cortex, the hippocampus, the basal ganglia and surrounding regions of three NHD patients by immunohistochemistry, using a panel of 16 antibodies (Table 1). The specificity of anti-TREM2 antibody (HPA010917) and anti-DAP12 antibody (sc-20783) utilized in the present study was carefully validated by Western blot analysis of protein extract derived from HEK293 cells expressing recombinant human TREM2 or DAP12 protein (Fig. 3a–c). Previous studies showed that both DAP12 and TREM2 are expressed predominantly in microglia in the normal human and mouse CNS.^{14–16} In control brains, we identified DAP12 immunoreactivity on the majority of ramified microglia (Fig. 4a) and an extremely small subset of cortical neurons but not on oligodendrocytes, whereas no DAP12-immunoreactive cells were detectable in NHD brains (Fig. 4b). Unexpectedly, TREM2 was not expressed on microglia but found on a small population of intravascular monocytes/macrophages and an extremely small subset of cortical neurons in control and NHD brains (Fig. 4c,d).

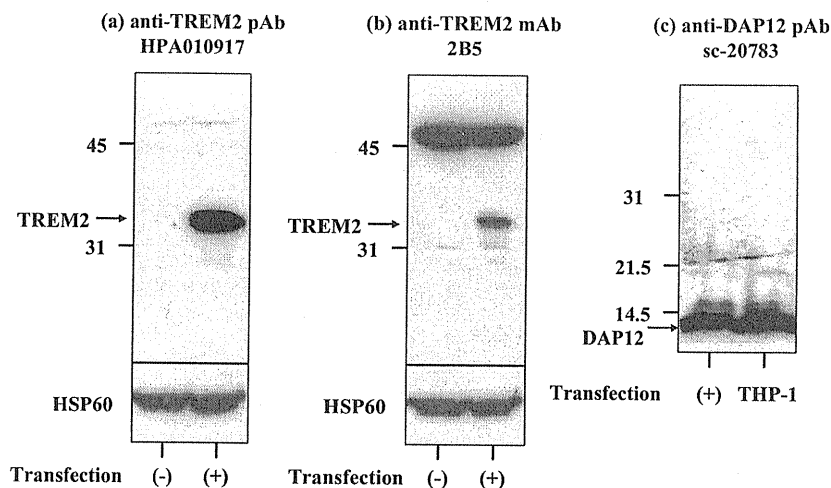


Fig. 3 Validation of antibody specificity by Western blot. The open-reading frame of the human triggering receptor expressed on myeloid cells 2 (TREM2) or DNAX-activation protein 12 (DAP12) gene was cloned in the expression vector pEF6-TOPO, and was transfected in HEK293 cells to express a nontagged recombinant TREM2 or DAP12 protein. Then, the protein extract was processed for Western blot analysis. The panels represent: (a) TREM2-expressing cells with anti-TREM2 pAb (HPA010917); (b) TREM2-expressing cells with anti-TREM2 mAb (2B5); and (c) DAP12-expressing cells with anti-DAP12 pAb (sc-20783). The blots in (a) and (b) were re-probed with anti-HSP60 antibody for an internal control (lower panels). The lanes indicate (-) nontransfected cells and (+) transfected cells. The left lane of the panel (c) represents the protein extract of THP-1 human monocytic leukemia cell line, serving as a positive control. It is evident that the anti-TREM2 mAb (2B5) reacts with a 47-kDa non-TREM2 protein (panel b).

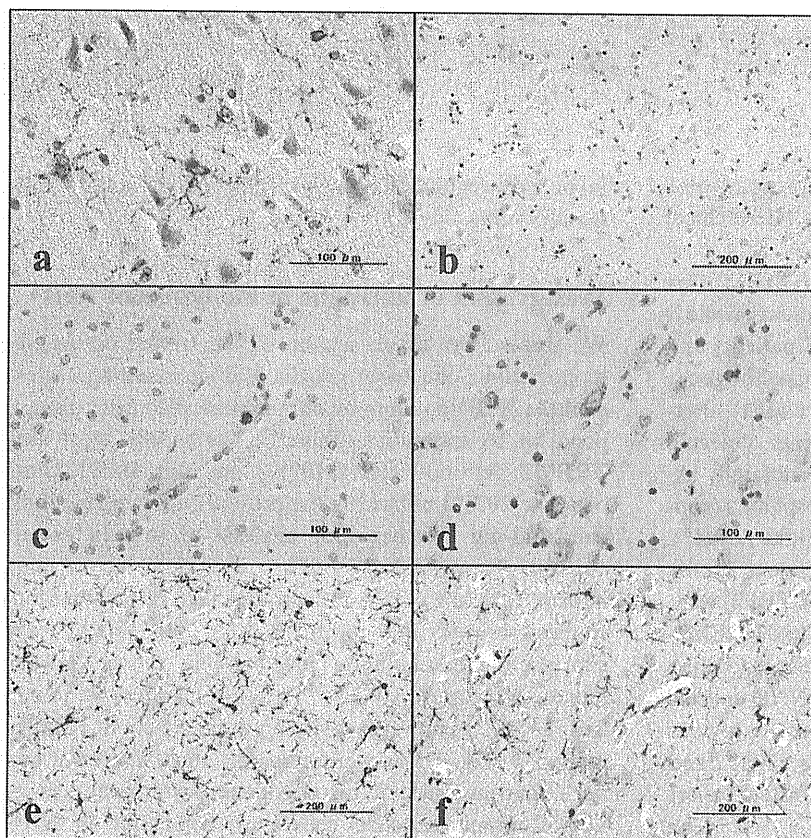


Fig. 4 DNAX-activation protein 12 (DAP12), triggering receptor expressed on myeloid cells 2 (TREM2), and Iba1 expression in Nasu-Hakola disease (NHD) and control brains. Formalin-fixed paraffin-embedded tissue sections of three NHD, four myotonic dystrophy (MD), and four non-neurological control (NC) brains were processed for immunohistochemistry with antibodies listed in Table 1. The panels represent: (a) NC1, the frontal cortex, DAP12; (b) NHD2, the basal ganglia, DAP12; (c) NC1, the frontal white matter, TREM2; (d) NHD3, the frontotemporal cortex, TREM2; (e) NC2, the hippocampus, Iba1; and (f) NHD1, the hippocampus, Iba1.